NUMERICAL ANALYSIS OF MULTIPLICITY AND TRANSITION PHENOMENON IN NATURAL CONVECTION

by

Hadi Kafil

B.S., Mechanical Engineering, Tabriz University, 2005

Submitted to the Institute for Graduate Studies in
Science and Engineering in partial fulfillment of
the requirements for the degree of
Master of Science

Graduate Program in Computational Science and Engineering

Boğaziçi University

2015

NUMERICAL ANALYSIS OF MULTIPLICITY AND TRANSITION PHENOMENON IN NATURAL CONVECTION

APPROVED BY:

Assoc. Prof. Ali Ecder .....
(Thesis Supervisor)

Prof. Dr. Can Özturan .....

Assist. Prof. Altuğ Başol .....

DATE OF APPROVAL: 29.09.2015

ACKNOWLEDGEMENTS

This thesis would not have been possible without the guidance and the help of various individuals who contributed their valuable assistance and support in the preparation and completion of this study.

Foremost, I owe my deepest gratitude to my thesis supervisor, Prof. Ali Ecder for his help, continuous support, guidance and patience throughout this study. I consider it an honor to work with him. I would also like to thank Prof. Dr. Can Özturan and Assist. Prof. Altuğ Başol for their interest, encouragement and helpful comments.

I am indebted to my friend Behrouz Haghgouyan who was always willing to help and give his best suggestion and advice. Last but not the least, I would like to thank my family for their kind support and great patience during my study.

ABSTRACT

NUMERICAL ANALYSIS OF MULTIPLICITY AND TRANSITION PHENOMENON IN NATURAL CONVECTION

This research is devoted to the numerical investigation of the transition and multiplicity phenomena in natural convection. The numerical simulation is performed for a 2-D closed domain using FLUENT, a commercial computational fluid dynamics package. In this study, the effects of different parameters such as Rayleigh number (Ra), aspect ratio (AR), and Prandtl number (Pr) are numerically analyzed. The complex phenomenon of onset of instability is studied to find the critical Ra numbers and bifurcation points. In a specific range of critical Ra numbers, transition and multiple results are observed using Rayleigh, boundary condition and pseudo-transient continuation methods. This method uses higher order temperature boundary conditions as an initial value on vertical walls. Multiple steady state results are observed at different Ra numbers. In a range of Ra numbers, the transition and multiple steady state results can completely change the convective flow pattern within the domain.

ÖZET

DOĞAL TAŞINIM GEÇİŞ VE ÇOKLUK OLGUSUNUN SAYISAL ANALİZİ

Bu araştırmada, doğal taşınım geçiş ve çokluk olguları sayısal olarak incelenmiştir. Sayısal simülasyon, iki boyutlu kapalı alan içinde ve FLUENT yazılımı kullanılarak yapılmıştır. Bu çalışmada, Rayleigh sayısı (Ra), en-boy oranı (AR) ve Prandtl sayısı (Pr) gibi farklı parametrelerin etkisi sayısal yöntemle analiz edilmiştir. Kritik Ra sayıları ve çatallanma noktalarını bulmak için, istikrarsızlık başlangıç olgusu incelenmiştir. Belirli bir kritik Ra sayı aralığı içinde, Ra ve sınır koşulları sürdürme yöntemini kullanarak, geçiş ve çokluk sonuçları gözlenmiştir.Bu yöntem yüksek mertebeli sıcaklık sınır koşullarını bir başlangıç değeri olarak dikey duvarlar üzerinde kullanıyor. Çoklu kararlı hal sonuçlari farklı Ra sayılarında gözlenmiştir. Belirli bir Ra sayı aralığı içinde, geçiş ve çoklu kararlı hal sonuçları, taşınım akış düzenini tamamen değişmesini göstermektedir.

TABLE OF CONTENTS

LIST OF FIGURES

LIST OF TABLES

LIST OF SYMBOLS

c_p	Specific heat capacity
D	mass diffusivity (m^2/s)
f_τ	typical frequency
g	Gravity
h	Enthalpy
H	Height
k	Thermal conductivity
L	Length
P	Pressure
P_0	Static pressure
p_d	Dynamic pressure
p^*	Dimensionless pressure
t	Time
t^*	Dimensionless time
T	Temperature
T_0	Operating temperature
T_{ref}	Reference temperature
T^*	Dimensionless temperature
u	Velocity in x-direction
v	Velocity in y-direction
u^*	Dimensionless velocity in x-direction
v^*	Dimensionless velocity in y-direction
α	Thermal diffusivity
β	Thermal expansion coefficient
β_T	Thermal expansion coefficient
β_C	compositional expansion coefficient
ΔT	Temperature differences
Δt	Time step

μ	Dynamic viscosity
ν	Kinematic viscosity
ρ	Density
ρ_0	Reference density of the flow(constant)
τ	Time constant

LIST OF ACRONYMS/ABBREVIATIONS

2D	Two Dimensional
3D	Three Dimensional
AR	Aspect Ratio
Ar	Archimedes number
BCs	Boundary Conditions
Bi	Biot number
Br	Brinkman number
Gr	Grashohf number
Gr_{cr}	Critical Grashohf number
ISPH	Incompressible smoothed particle hydrodynamics
Le	Lewis number
Nu	Nusselt number
Pr	Prandtl number
Ra	Rayleigh number
Ra_{cr}	Critical Rayleigh number
Re	Reynolds number
Sc	Schmidt number
Sh	Sherwood number
SPH	Smoothed particle hydrodynamics

1. INTRODUCTION

Heat transfer occurs within a system in the presence of a temperature gradient. Natural convection is a type of heat transfer, which is induced by buoyancy force, without any external forcing condition. In other words, the fluid motion originates from body force when the density gradient is due to the temperature gradient.

Natural convection plays an important role in increasing heat transfer within the system. In recent years, natural convection received considerable interest in various fields such as new electronic devices, solar thermal receiver systems, solidification process [4], and biomedical [5]. In some systems, on the contrary, natural convection has drawback effects when it provides resistance to heat transfer or affect the interface of solid/liquid. It can happen in crystal growth or in fluid flow through the pipe. In order to better identification of natural convection, it needs be examined profoundly. This problem reveals a variety of complex behaviors and high sensitivity to small variations of parameters, such as the aspect ratio (AR), Rayleigh number (Ra), Prandtl number (Pr), and the thermal boundary conditions (BC). Ra number plays a significant role in the most of the natural convection investigation. The onset of instability and bifurcation happen in a range of determined Ra numbers.

Despite the fact that there is a density differences within the domain, by the Boussinesq approximation as introduced by Joseph Valentin Boussinesq (1842–1929) [6] a French mathematician and physicist known for advances in fluid dynamics, the density is assumed to be constant except for the body forces. More than one hundred years ago, in 1903 Joseph Valentin Boussinesq [7] observed that: "The variations of density can be ignored except where they are multiplied by the acceleration of gravity in equation of motion for the vertical component of the velocity vector."

The transition natural convection was observed in melt flow by Hurle [4]. The severe effects of natural convection on melt flow have motivated recent studies to examine convective flow [8]. The natural convection in melt flow affects the process of

crystallization, and it completely affects the interface and crystal formation, and it strongly changes the solute and temperature distribution within the melt flow [9].

1.1. Literature Review

At specific Ra number (bifurcation point), the transition from conduction (Nu=1) to convection (onset of convective instability) occurs. The first observation of transition and unstable natural convection phenomenon happened in experimental researches by Hurle(1966) [4, 10]. The unstable natural convection has been specifically studied in some researches [11–13] for two dimensional (2D) and three dimensional (3D) cavities. However, these studies were performed for variation of Pr numbers, which are not of practical use. In addition, the onset of unstable natural convection has been analyzed in Gelfagt *et al.* studies [14, 15]. Their study focuses on onset of instability phenomena in convective fluid flow for different AR. They proposed that the Pr number and the AR play a significant role in steadily transient natural convection. They investigated at various critical Grashof number and aspect ratios, and drew the graph which showed the different results by increasing AR.

A recent approach, which studied the natural convection by using ISPH method, was introduced by Danis *et al.* [16]. ISPH method was used to simulate natural convection in a square cavity with Boussinesq approximation at Ra numbers between 10^3 and 10^6. Despite the fact that the SPH has been always used to discretize the Lagrangian equations, in this study the uniform Eulerian grids is discretized using SPH operators. In other meshless Lagrangian method, the SPH particles are moving inside the domain, but in this approach SPH particles are kept stationary. Since all particles are stationary, the Eulerian form of governing equations is used instead of the Lagrangian form of equations. In addition, they have used an incompressible approach, which is called Incompressible SPH (ISPH). Moreover, ISPH method was used to prevent the density error accumulation and particle disordering. In this method, the incompressibility is directly imposes an intermediate velocity field, which is obtained without considering gradient of pressure.

The analyze of different bifurcation points and multiple solutions was examined by Ventury *et al.* [1]. In his study, deterministic analysis was used to capture steady-state solutions and primary bifurcations, where multiple stable solutions were found within specific ranges of Ra number. Finally, the stochastic analysis was carried out on random initial condition flows around bifurcation points to analyze the transient natural convection behavior.

All probable convective flow patterns were investigated by Puigjaner et al. [2]. All stable and unstable flow patterns for Rayleigh-Benard convection problem with Pr=0.7 at different Ra numbers were investigated by using parameter continuation techniques. Multiple convection flow pattern can observe even for moderate Ra numbers. The different patterns were discussed by streamlines direction and number of convection rolls and its different shapes.

Sheu *et al.* [17] discussed the transient convection and the onset of bifurcation point in a 3D model, which is numerically demonstrated that a unique symmetric and steady-state solution exists in small Ra number. As the Ra increases beyond onset of bifurcation point, the symmetric results become asymmetric. After one point (bifurcation point), two different solutions can be obtained. Analysis of transition to oscillator convection for 2D and 3D domain with low Pr number was investigated by Henry et al. (1998) [13]. In this study, different convective flow pattern was observed for Pr=0 and a non-zero Pr number case.

Various numerical studies have been performed on the instability of steady and transient natural convective flows. Mercader *et al.* [18] studied the parametric variation, BC, and periodic analysis. Firstly, they analyzed the basic state and its primary bifurcation that has two cases of temperature BCs, which are performed in horizontal plates with Pr= 0.007 with rectangular cavity of AR=2. Furthermore, periodic analysis was considered in their research, in which they studied both steady and transient convective flow. Finally, it was observed that by increasing thermal effects, secondary bifurcations revealed for both temperature profile cases.

The oscillatory convection within the liquid phase of two-phase flow was observed [4, 9, 10], and some numerical and experimental studies [14, 19] investigated the oscillatory natural convection. Although these studies identify the phenomenon, a complete analysis that can cover the bifurcation points and multiple results is still lacking. In addition, It was mentioned that at critical Ra number, the transition and oscillatory natural convection intensively affect the fluid flow within closed domain. Joo-Sik Yoo [20] studied the combined effect of thermal and hydrodynamic instability natural convection in a narrow horizontal concentric annulus with Pr=0.4. The multiple natural convection patterns were shown in his investigation within annular gap between two concentric cylinder. The results represented the complicated multicellular flow. Increasing Ra number changes the multicellular flow to a nearly monocellular structure. Periodic steady solutions were observed within higher range of Ra numbers.

According to the literature, it is still uncertain why crystal growth of some materials is easy and for others it is not [19, 21]. It has been neglected that at the low Pr numbers ($Pr < 0.1$), the oscillatory natural convection flow occurs at the range of Ra numbers which are so close to the experimental conditions [21]. The strength of fluid flow and the unstable transition natural convection can strongly change the interface of two-phase flow. The effects of multiplicity and transition of natural convection has been neglected to estimate the shape and movement of the solid/liquid interface of two-phase flow [19]. The effects of BC and specially temperature gradient are investigated by Erenburg et al. [22]. Partially heated walls are set up as boundary condition to analyze the multiplicity and bifurcations of natural convection. In this research, both continuous and partial temperature gradient on wall are considered. Selver et al. [19] studied the partial heated vertical walls to simulate the floating-zone crystal growth.

Most of the studies, which discuss oscillatory convection, were considered the thermocapillary effects for upper BC on fluid flow [23]. The buoyancy force is the dominant force to carry out the natural convection in closed domain; however, the influence of thermocapillary forces on buoyancy-driven convection cannot be ignored. This influences were numerically studied for open cavities with differentially heated walls [24]. In these studies the Reynolds number (Re) is also important because they

used the Marangoni stress to solve the stress-free (open) BC. Thermocapillary can impose intensive effects on buoyancy-driven flow. The results of combination of these two forces can completely change the stability of natural convection within the domain.

Some studies used the thermal lattice Boltzmann method to study the natural convection [25–27]. In this method, instead of using finite difference, finite element and finite volume methods to solve Naiver–Stokes equations, the lattice Boltzmann method were employed. In addition, there are some new combinations of lattice Boltzmann method with other methods to create new explicit method [28], which is based on the lattice Boltzmann method (LBM) combined with Taylor series expansion and the least squares approach.

Most of natural convection studies were used Boussinesq approximation to simulate the convective flow. However, there are several studies which used non-Boussinesq assumption to model convective flow, Hamimid et al. [29] was used the time dependent Naiver–Stokes equations under the Low Mach Number approximation (LMN method). This investigation demonstrated that for large temperature differences, LMN compressible method obtained better results for convective flow. In addition, Vekstein (2004) [30] investigated natural convection without using Boussinesq approximation, considered the energy of liquid and gas to investigate the onset of convective instability. In this study, the onset of natural convection instability is discussed by energy of the fluid. In other words, a gravitational energy sustains the fluid flow in natural convection by interchanging a hotter fluid with less density to cooler one with more density. The distinguish convection instability between fluid and ideal gas was also discussed in this research. Unlike a gas, a liquid may be considered as almost incompressible fluid. This means that its density, in the general case, is a function of pressure and temperature $\rho = \rho(P, T)$. But since it has a very weak dependence on the pressure, one may simply consider $\rho = \rho(T)$.

Szewc et al. [31] discussed the Boussinesq approximation failure by using SPH method, in which natural convection in a square cavity with a Boussinesq and a non-Boussinesq formulation was studied. In significant differences of density due to temper-

ature gradient, the dimensionless Gay-Lussac number is suggested to measure density gradient in non-isothermal flows. The effect of Gay-Lussac number was investigated for velocity field and Nusselt number of non-Boussinesq convective flow on their study.

When both heat and mass transfer affect natural convection, the double-diffusive convective flow is defined to solve the problem [32]. For multi-component mixing flows, the transport of enthalpy, due to species diffusion, can have a significant effect on the enthalpy field and should not be neglected. Lewis number ($Le = \frac{k}{\rho c_p D}$) is very important in these kinds of investigation; when the Le number for any species $Le \gg 1$ increase, the thermo-solutal effects become so significant to simulate the convective flow [33].

The effects of rotating flow on oscillatory natural convection was studied experimentally and numerically [34–36] . For specific range of Gr numbers, thermal oscillations are detected at several rotation rate. In addition, it is found that the frequency of oscillation is a function of the Gr number.

2. MATHEMATICAL MODELING

The fluid motion with temperature effects results in governing equations in which natural convection plays a major role by buoyancy forces, and the buoyancy forces sustain the fluid flow. The fluid is assumed Newtonian and quasi-incompressible (Boussinesq approximation), and the Navier-Stokes equations coupled with the energy equation govern the flow with the constant physical properties except in the buoyancy term where ρ is taken as a linear function of the temperature. The equations for conservation of mass, momentum, and energy [28, 37, 38] can be written as follows:

$$\frac{\partial u}{\partial x} + \frac{\partial v}{\partial y} = 0 \tag{2.1}$$

$$\frac{\partial u}{\partial t} + u\frac{\partial u}{\partial x} + v\frac{\partial u}{\partial y} = -\frac{1}{\rho_0}(\frac{\partial P}{\partial x}) + \nu(\frac{\partial^2 u}{\partial x^2} + \frac{\partial^2 u}{\partial y^2}) \tag{2.2}$$

$$\frac{\partial v}{\partial t} + u\frac{\partial v}{\partial x} + v\frac{\partial v}{\partial y} = -\frac{1}{\rho_0}(\frac{\partial P}{\partial y}) + \nu(\frac{\partial^2 v}{\partial x^2} + \frac{\partial^2 v}{\partial y^2}) - g \tag{2.3}$$

$$\frac{\partial T}{\partial t} + u\frac{\partial T}{\partial x} + v\frac{\partial T}{\partial y} = \alpha(\frac{\partial^2 T}{\partial x^2} + \frac{\partial^2 T}{\partial y^2}) \tag{2.4}$$

2.1. Natural Convection

The natural convection within the closed domain can be modeled in one of the following ways:

- In small temperature gradient within the domain, the density can be assumed constant except in buoyancy term of momentum equation (Boussinesq Approximation). This approach is valid when $\beta\Delta T \ll 1$.
- For high temperature differences within the domain, a constant density assumption can not be correct, and the fluid flow is considered compressible flow.

2.1.1. Boussinesq Approximation

In Bossinessq approximation, the fluid density is defined as a function of temperature and thus the temperature-field is coupled with the flow-field. This problem is assumed the no-slip boundary condition with constant properties except for the body force term in the momentum Equations 2.3.

In moderate temperature differences, the Taylor series expansion of density (ρ) is written around the referance density ρ_0 :

$$\rho = \rho_0 + (\frac{\partial \rho}{\partial T})_p (T - T_0) + (\frac{\partial^2 \rho}{\partial T^2})_p (T - T_0)^2 + ... \tag{2.5}$$

In this temperature gradient the density changes is assumed linear; therefore the nonlinear part of Taylor series is ignored. The thermal expansion coefficient (isobaric) β is introduced as:

$$\beta = -\frac{1}{\rho_0}(\frac{\partial \rho}{\partial T})_P \tag{2.6}$$

Thus as a result the above explanation:

$$(\rho - \rho_0) \approx \rho_0 \beta (T - T_0) \tag{2.7}$$

The natural convection in which both mass and energy is driven by buoyancy due to simultaneous temperature and concentration gradients, is called double diffusive or thermo-solutal convection [8] Thermal and solutal gradients cause to complex flow structures, a thermal expansion coefficient β_T is defined:

$$\beta_T = -\frac{1}{\rho}(\frac{\partial \rho}{\partial T}) \tag{2.8}$$

As we study the behaviour of homogeneous (one-component) fluids, corresponding to a liquid pure material (small Prandtl number) therefore to define the buoyancy term in momentum equation ($\beta_T = \beta$ is assumed).

The pressure gradient in y-direction consist of hydrostatic pressure ($-\rho g$) and the dynamic pressure which is the pressure of a fluid motion ($-\frac{\partial p_d}{\partial y}$). Thus, the pressure gradient term in equation 2.4 is rewritten as:

$$-(\frac{\partial P}{\partial y}) = -(-\rho g + \frac{\partial p_d}{\partial y}) \tag{2.9}$$

Consequently, we replace above term instead of pressure term in eq. 2.4 and obtain the final form of momentum equation in y-direction by assuming Boussinesq approximation.

$$\rho_0 u\frac{\partial v}{\partial x} + \rho_0 v\frac{\partial v}{\partial y} = -(-\rho g + \frac{\partial p_d}{\partial y}) + \mu(\frac{\partial^2 v}{\partial x^2} + \frac{\partial^2 v}{\partial y^2}) - \rho_0 g \tag{2.10}$$

$$\implies \rho_0 u\frac{\partial v}{\partial x} + \rho_0 v\frac{\partial v}{\partial y} = -\frac{\partial p_d}{\partial y} + \mu(\frac{\partial^2 v}{\partial x^2} + \frac{\partial^2 v}{\partial y^2}) + (\rho - \rho_0)g \tag{2.11}$$

$$\implies u\frac{\partial v}{\partial x} + v\frac{\partial v}{\partial y} = -\frac{1}{\rho_0}\frac{\partial p_d}{\partial y} + \nu(\frac{\partial^2 v}{\partial x^2} + \frac{\partial^2 v}{\partial y^2}) + g\beta(T - T_0) \tag{2.12}$$

where ρ_0 is the constant density (reference density) of the flow, T_0 is the operating temperature, and β is the thermal expansion coefficient. In this equation T is the temperature distribution within the domain which is obtained from energy equation. Equation 2.12 is obtained by using the Boussinesq approximation $\rho = \rho_0(1 - \beta\Delta T)$ to eliminate ρ from the buoyancy term. This approximation is accurate as long as changes in actual density are small; specifically, the Boussinesq approximation is valid when $\beta(T - T_0) \ll 1$.

In addition, there is no hydrostatic pressure in x-direction; thus the pressure

gradient is due to fluid motion.

$$\frac{\partial P}{\partial x} = \frac{\partial p_d}{\partial x} \tag{2.13}$$

We elimnate the 'd' index in both pressure gradient terms to simplify the equations. Therefore, the final form of equations 2.3 and 2.4 by considering the Boussinesq approximation and time independent problem are rewritten:

$$u\frac{\partial u}{\partial x} + v\frac{\partial u}{\partial y} = -\frac{1}{\rho_0}(\frac{\partial p}{\partial x}) + \nu(\frac{\partial^2 u}{\partial x^2} + \frac{\partial^2 u}{\partial y^2}) \tag{2.14}$$

$$u\frac{\partial v}{\partial x} + v\frac{\partial v}{\partial y} = -\frac{1}{\rho_0}\frac{\partial p}{\partial y} + \nu(\frac{\partial^2 v}{\partial x^2} + \frac{\partial^2 v}{\partial y^2}) + g\beta(T - T_0) \tag{2.15}$$

2.1.2. Energy equation

The basic form of Energy equation which is solved in general problems in FLUENT [37] is as follows:

$$\frac{\partial(\rho E)}{\partial t} + \nabla.(\vec{v}(\rho E + p)) = \nabla.(k\nabla T - \sum hJ + (\tau.\vec{v})) + S_h \tag{2.16}$$

Energy E per unit mass is defined as:

$$E = h - \frac{P}{\rho} + \frac{V^2}{2} \tag{2.17}$$

This problem does not depend on time; therefore the first term is eliminated. The differences in pressure and kinetic energy are small in incompressible. Thus, for our case the derivatives of them are assumed zero, and h is refers to sensible enthalpy:

$$h = \int_{T_{ref}}^{T} c_p dT \tag{2.18}$$

The reference temperature in sensible enthalpy calculation is set to 298.15 K

In equation 2.16 $\sum hJ$ is for species diffusion and $\tau.\vec{v}$ is for viscous dissipation. Both parts are eliminated. In our natural convection, the material is assumed pure and therefore the species diffusion is ignored. The Viscous dissipation, also called viscous heating, is used for high-velocity compressible flows and high shear stress in fluids (e.g. lubrication). The viscous dissipation plays an important role in energy aquation when the Brinkman number approaches or exceeds unity.

$$Br = \frac{\mu {U_e}^2}{k\Delta T} \tag{2.19}$$

There is no energy source S_n in our problem; therefore it is negligible in the equation 2.16. Finally, the 2-D energy equation is derived from 2.16

$$\nabla.(\vec{v}(\rho E) = \nabla.(k\nabla T) \tag{2.20}$$

$$\nabla.(\vec{v}(\rho c_p T) = \nabla.(k\nabla T) \tag{2.21}$$

$$\rho c_p \nabla.(\vec{v}.T) = k\nabla.(\nabla T) \tag{2.22}$$

and then,

$$u\frac{\partial T}{\partial x} + v\frac{\partial T}{\partial y} = \alpha(\frac{\partial^2 T}{\partial x^2} + \frac{\partial^2 T}{\partial y^2}) \tag{2.23}$$

2.2. Dimensionless Formulation

In order to non-dimensionalize the governing equations, the dimensionless parameters are defined [17, 38, 39]:

$$x^* = \frac{x}{L}, y^* = \frac{y}{L}$$

$$u^* = \frac{uL}{\alpha}, v^* = \frac{vL}{\alpha}$$

$$T^* = \frac{T - T_0}{T_H - T_C}$$

$$t^* = \frac{t\alpha}{L}$$

$$p^* = \frac{pL^2}{\rho\alpha^2}$$

By assuming the above dimensionless parameters, we want to derive the dimensionless form of the following equations.

$$\frac{\partial u}{\partial x} + \frac{\partial v}{\partial y} = 0 \tag{2.24}$$

$$u\frac{\partial u}{\partial x} + v\frac{\partial u}{\partial y} = -\frac{1}{\rho_0}\frac{\partial p}{\partial x} + \nu(\frac{\partial^2 u}{\partial x^2} + \frac{\partial^2 u}{\partial y^2}) \tag{2.25}$$

$$u\frac{\partial v}{\partial x} + v\frac{\partial v}{\partial y} = -\frac{1}{\rho_0}\frac{\partial p}{\partial y} + \nu(\frac{\partial^2 v}{\partial x^2} + \frac{\partial^2 v}{\partial y^2}) + g\beta(T - T_0) \tag{2.26}$$

$$u\frac{\partial T}{\partial x} + v\frac{\partial T}{\partial y} = \alpha(\frac{\partial^2 T}{\partial x^2} + \frac{\partial^2 T}{\partial y^2}) \tag{2.27}$$

The Equations 2.24 and 2.25 are written by using the dimensionless parameters:

$$\frac{\partial(\frac{u^*\alpha}{L})}{\partial(x^*L)} + \frac{\partial^{(\frac{v^*\alpha}{L})}}{\partial(y^*L)} = \frac{\alpha}{L^2}(\frac{\partial u^*}{\partial x^*} + \frac{\partial v^*}{\partial y^*}) = \frac{\partial u^*}{\partial x^*} + \frac{\partial v^*}{\partial y^*} = 0 \tag{2.28}$$

$$\begin{aligned}(\frac{u^*\alpha}{L})\frac{\partial(\frac{u^*\alpha}{L})}{\partial(x^*L)} + (\frac{v^*\alpha}{L})\frac{\partial(\frac{u^*\alpha}{L})}{\partial(y^*L)} &= -\frac{1}{\rho_0}\frac{\partial(\frac{p^*\rho\alpha^2}{L^2})}{\partial(x^*L)} + \nu(\frac{\partial^2(\frac{u^*\alpha}{L})}{\partial(x^*L)^2} + \frac{\partial^2(\frac{u^*\alpha}{L})}{\partial(y^*L^2)}) \\ \implies \frac{\alpha^2}{L^3}(u^*\frac{\partial u^*}{\partial x^*} + v^*\frac{\partial u^*}{\partial y^*}) &= -\frac{\rho}{\rho_0}(\frac{\alpha^2}{L^3})\frac{\partial p^*}{\partial x^*} + \frac{\nu\alpha}{L^3}(\frac{\partial^2 u^*}{\partial x^{*2}} + \frac{\partial^2 u^*}{\partial y^{*2}})\end{aligned} \tag{2.29}$$

In Equation 2.29 $\frac{\rho}{\rho_0}$ is non-dimension, and by multiplying both sides by $\frac{L^3}{\alpha^2}$, and dimensionless number (Pr number) which is defined as ratio of momentum diffusivity to

thermal diffusivity is defined as following:

$$\nu = \frac{\mu}{\rho} \tag{2.30}$$

$$\alpha = \frac{k}{\rho c_P} \tag{2.31}$$

$$Pr = \frac{\nu}{\alpha} = \frac{c_P \mu}{k} \tag{2.32}$$

Therefore, the momentum equation in x-direction is derived:

$$u^* \frac{\partial u^*}{\partial x^*} + v^* \frac{\partial u^*}{\partial y^*} = -\frac{\partial p^*}{\partial x^*} + Pr(\frac{\partial^2 u^*}{\partial x^{*2}} + \frac{\partial^2 u^*}{\partial y^{*2}}) \tag{2.33}$$

For momentum equation in y-direction:

$$\begin{aligned} (\frac{u^* \alpha}{L}) \frac{\partial (\frac{v^* \alpha}{L})}{\partial (x^* L)} + (\frac{v^* \alpha}{L}) \frac{\partial (\frac{v^* \alpha}{L})}{\partial (y^* L)} &= -\frac{1}{\rho_0} \frac{\partial (\frac{p^* \rho \alpha^2}{L^2})}{\partial (y^* L)} + \nu (\frac{\partial^2 (\frac{v^* \alpha}{L})}{\partial (x^* L)^2} + \frac{\partial^2 (\frac{v^* \alpha}{L})}{\partial (y^* L^2)}) + g\beta T^* \Delta T \\ \frac{\alpha^2}{L^3} (u^* \frac{\partial v^*}{\partial x^*} + v^* \frac{\partial v^*}{\partial y^*}) &= -\frac{\rho}{\rho_0} (\frac{\alpha^2}{L^3}) \frac{\partial p^*}{\partial y^*} + \frac{\nu \alpha}{L^3} (\frac{\partial^2 v^*}{\partial x^{*2}} + \frac{\partial^2 v^*}{\partial y^{*2}}) + g\beta T^* \Delta T \end{aligned} \tag{2.34}$$

In this equation, $\frac{\rho}{\rho_0}$ is non-dimension and after multiplying both sides to $\frac{L^3}{\alpha^2}$, and multiply the last term of Equation 2.34 to $\frac{\nu}{\nu}$:

$$Ra = \frac{g\beta \Delta T L^3}{\nu \alpha} = \frac{\rho^2 c_P g \beta \Delta T L^3}{\mu k} \tag{2.35}$$

$$Ra = Gr.Pr \tag{2.36}$$

$$u^* \frac{\partial v^*}{\partial x^*} + v^* \frac{\partial v^*}{\partial y^*} = -\frac{\partial p^*}{\partial y^*} + \frac{\nu}{\alpha} (\frac{\partial^2 v^*}{\partial x^{*2}} + \frac{\partial^2 v^*}{\partial y^{*2}}) + (\frac{\nu}{\alpha})(\frac{g\beta \Delta T L^3}{\nu \alpha}) T^* \tag{2.37}$$

the momentum equation in y-direction is derived:

$$u^* \frac{\partial v^*}{\partial x^*} + v^* \frac{\partial v^*}{\partial y^*} = -\frac{\partial p^*}{\partial y^*} + Pr(\frac{\partial^2 v^*}{\partial x^{*2}} + \frac{\partial^2 v^*}{\partial y^{*2}}) + RaPrT^* \tag{2.38}$$

The Equations 2.27 is written by using the dimensionless parameters as following:

$$\begin{aligned}(\frac{u^*\alpha}{L})\frac{\partial T^*}{\partial(x^*L)} + (\frac{v^*\alpha}{L})\frac{\partial T^*}{\partial(y^*L)} &= \alpha(\frac{\partial^2 T^*}{\partial(x^*L^2)} + \frac{\partial^2 T^*}{\partial(y^*L^2)}) \\ \implies \frac{\alpha}{L^2}(u^*\frac{\partial T^*}{\partial x^*} + v^*\frac{\partial T^*}{\partial y^*}) &= \frac{\alpha}{L^2}(\frac{\partial^2 T^*}{\partial x^{*2}} + \frac{\partial^2 T^*}{\partial y^{*2}}) \end{aligned} \tag{2.39}$$

By multiplying both sides to $\frac{L^2}{\alpha}$, the non-dimensionalized energy equation is derived:

$$u^*\frac{\partial T^*}{\partial x^*} + v^*\frac{\partial T^*}{\partial y^*} = (\frac{\partial^2 T^*}{\partial x^{*2}} + \frac{\partial^2 T^*}{\partial y^{*2}}) \tag{2.40}$$

Therefore, all non-dimensionized equations are as following:

$$\frac{\partial u^*}{\partial x^*} + \frac{\partial v^*}{\partial y^*} = 0 \tag{2.41}$$

$$\frac{\partial u^*}{\partial t^*} + u^*\frac{\partial u^*}{\partial x^*} + v^*\frac{\partial u^*}{\partial y^*} = -\frac{\partial p^*}{\partial x^*} + Pr(\frac{\partial^2 u^*}{\partial x^{*2}} + \frac{\partial^2 u^*}{\partial y^{*2}}) \tag{2.42}$$

$$\frac{\partial v^*}{\partial t^*} + u^*\frac{\partial v^*}{\partial x^*} + v^*\frac{\partial v^*}{\partial y^*} = -\frac{\partial p^*}{\partial y^*} + Pr(\frac{\partial^2 v^*}{\partial x^{*2}} + \frac{\partial^2 u^*}{\partial y^{*2}}) + RaPrT^* \tag{2.43}$$

$$u^*\frac{\partial T^*}{\partial x^*} + v^*\frac{\partial T^*}{\partial y^*} = (\frac{\partial^2 T^*}{\partial x^{*2}} + \frac{\partial^2 T^*}{\partial y^{*2}}) \tag{2.44}$$

At lower Ra number the behaviour of fluid is steady, but in higher Ra number the fluid shows turbulence. Onset of transition in natural convection is occurred in a range of critical Ra numbers.

The importance of buoyancy forces in a mixed convection flow can be measured by the ratio of the Grashof and Reynolds numbers.

$$\frac{Gr}{Re^2} = \frac{g\beta\Delta TL}{\nu^2} \tag{2.45}$$

When this ratio exceeds unity, the buoyancy effect is dominant, and the natural convection is occurred. Conversely, if it is very small, buoyancy forces is weak and can be ignored. In pure natural convection, the strength of the buoyancy-induced flow is measured by the Ra number.

2.3. Problem definition

The Rayleigh-Benard convection occurs in a volume of fluid that is heated from below. The hotter fluid (at the bottom) get a higher temperature and therefore a lower density than the rest of the fluid. Gravity tends to draw down the colder and heavier fluid at the top but this is opposed by the viscous force in the fluid. Rayleigh-Benard convection is an example of thermal instability where temperature difference between the top and bottom caused by heating the fluid from below results in formation of rolls. If the temperature gradient, and thus the density gradient, is large enough the gravitational forces will dominate and instability will occur. Rayleigh-Benard instability has been a topic for many experimental and numerical studies [40]. The Rayleigh-Benard convection occurs in a volume of fluid that is heated from below and it is known as the Rayleigh-Benard instability. The viscous force and gravitational force within the fluid are in challenging. The balance between these two forces determines that the convection will occur or not. If the temperature gradient, density gradient, was large enough, the gravitational forces will dominate and instability will occur. The Rayleigh-Benard instability develops when Ra number is above a critical value. The Rayleigh-Benard convection problem domain is shown in Figure 2.1. The effect of domain geometry is analysed by AR, which is actually the ratio of height to length (AR=H/L), as depicted in Figure 2.1. Different aspect ratio(AR=1/4, 1/2, 1, 2, and 4) are considered in this research. The problem is defined using constant temperature at the top and the bottom. Insolated BC is defined on sidewalls which is depicted in Figure 2.1.

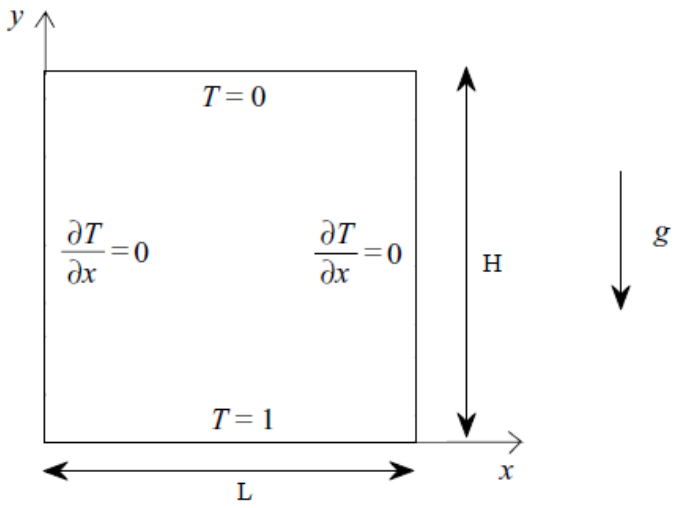

Figure 2.1. The Rayleigh-Benard domain geometry and temperature BCs; The sidewalls are assumed adiabatic and the horizontal walls are set to constant temperature.

3. Computational Modeling

3.1. Numerical method to solve the problem

The ANSYS FLUENT 14 [41] is used to solve the problem. This commercial program is based on finite volume discritization method. The Rayleigh-Benard natural convection problem is a nonlinear and unstable problem. In this problem, temperature BC and temperature initial values are very important. First of all, the energy equation is solved to obtain an initial temperature distribution which is used in momentum equation as an initial value. It is difficult the convergence of non-linear part of momentum equation because of the intense convective flow. At low Ra numbers, the SIMPLE method [42] is utilized for all AR.

(i) For low Ra number, the SIMPLE scheme is used for Pressure-Velocity Coupling
(ii) For the problem with the Rayleigh number higher than critical Ra number the COUPLED scheme combined with pseudo-transient method is applied.

The spatial discretization for all Ra number is the same and it is briefly explained as follows. To solve governing partial differential equations (PDEs) numerically, which are defined in previous chapter, the finite volume method is used to discretized the domain into finite set of control volumes or cells. The Finite volume discretization is explained briefly as follows.

The natural convection problem in closed domain is solved by steady convection-diffusion equation which can be derived from the general transport equation. General transport equation for mass, momentum, and energy is applied to each cell. For a general property ϕ by eliminating the unsteady part, the integration over the control volume is derived as follows.

$$\int_A \rho\phi\vec{v}dA = \int_A \Gamma grad\phi)dA + \int_{CV} S_\phi dV \tag{3.1}$$

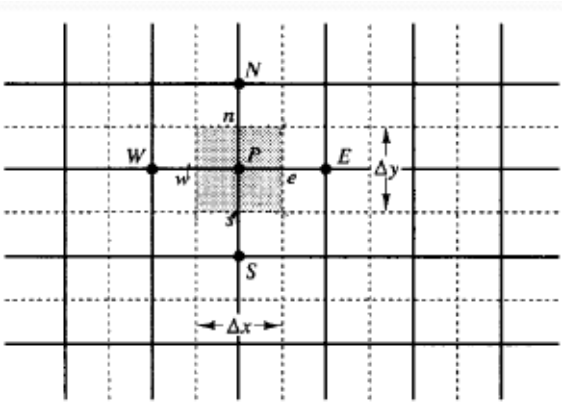

Figure 3.1. Two-dimensional grid.

This equation is applied to each control volume, or cell, in the computational domain. The flux balance in control volume is represented in this equation. The left side gives the net convective flux and the right side derives the net diffusive flux plus the generation of the property ϕ.

The equation 3.1 is discretized into algebraic form. For cell p, it is written as

$$\sum_{faces} \rho_f \vec{v}_f \phi_f \vec{A}_f = \sum_{faces} \Gamma_\phi \nabla \phi_f . \vec{A}_f + S_\phi V \tag{3.2}$$

There are unknown variables in equation 3.2 at the cell center and neighbor cells.

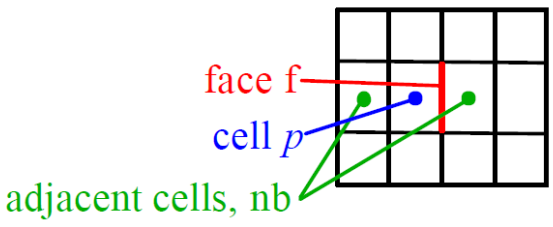

Figure 3.2. Control cell of 2D domain

Then, this equation is non-linear with respect to these variables. A linearized form of

Equation 3.2 can be written as:

$$a_P\phi = \sum_{nb} a_{nb}\phi_{nb} + b \tag{3.3}$$

where the subscript nb refers to neighbor cells, a_p and a_{nb} are the linearized coefficients for ϕ and ϕ_{nb} , and b is the contribution of the constant part of the source term S_ϕ. To solve the problem with the Ra number higher than critical Ra number Coupled and Pseudo-Transient methods are applied.

For convection-diffusion problems, the upwind differencing scheme has better accuracy in comparison to the central scheme because the upwind schem is able to identify the flow direction that is practical in a strongly convective flow. FLUENT stores the value of ϕ at the cell centers, but for the convection terms the face value ϕ_f is required which must be interpolated from the cell center values. This is accomplished using an upwind scheme. In this problem, the second-Order Upwind Scheme is used to discretize the momentum, energy, and pressure values.

3.1.1. Second-Order Upwind Scheme

Considering the first-order upwind is selected the face value ϕ_f equal to the cell-center value of ϕ in the upstream cell [41]. The second-Order upwinding is added to the second part of Taylor series expansion to compute the face value ϕ_f using the following expression:

$$\phi_f = \phi + \nabla\phi.\vec{r} \tag{3.4}$$

Therefore, the face value is calculated by the cell-centered value ϕ and its gradient$\nabla\phi$ and the distance vector $\vec{r}$ between cell center and the face.

The determination of gradient of the scaler value ϕ needs a method to calculate the derivation. The Least Squares Cell-Based method is used in all calculations.

3.1.2. Least Squares Cell-Based Method

Gradients are needed not only for obtaining the value of ϕ at the face, but also for computing secondary diffusion terms and velocity derivatives. To calculate the cell value between c_0 and c_i with the distance vector δr_i and the direction from c_0 to c_i can be represented as

$$(\nabla\phi)_{c0} = \frac{(\phi_{ci} - \phi_{c0})}{\Delta r_i} \tag{3.5}$$

3.2. Discretization of the Governing Equations

The three main governing equations (steady-state continuity, momentum, and energy) are written in integral form:

$$\oint \rho\vec{v}.d\vec{A} = 0 \tag{3.6}$$

$$\oint \rho\vec{v}\vec{v}.d\vec{A} = \oint (\mu\nabla\vec{v}).d\vec{A} - \int \rho_0\beta\vec{g}(\vec{T} - T_0)dV \tag{3.7}$$

By setting $\phi = v$ in equation 3.3, the discretized form for y-momentum equation is obtained:

$$a_P v = \sum_{nb} a_{nb} v_{nb} + \sum P_f A \tag{3.8}$$

The pressure field and face mass fluxes are unknown. There are different methods to obtain the pressure field; these are explained in next section.

Pressure and velocity are both stored in cell centers. However, Equation 3.8 requires the value of the pressure at the face between cells $c0$ and $c1$. Therefore, an interpolation scheme is required to compute the face values of pressure from the cell values.

3.2.1. Pressure Interpolation Schemes

The second-order scheme reconstructs the face pressure in the manner used for second-order accurate convection terms (see 3.1.1). This scheme may provide some improvement over the standard and linear schemes, but it may cause some trouble if it is used at the start of a calculation and/or with a bad mesh.

For high Ra numbers, the body Force Weighted method is applied as a pressure solver. The body-force-weighted scheme computes the face pressure by assuming that the normal gradient of the difference between pressure and body forces is constant.

In very-high-Rayleigh-number natural convection flows where density or momentum equations is strongly coupled with temperature, it is recommended to use the under-relaxation factor for the energy equation less than 1.0.

3.3. Mesh sensitivity

To examine the mesh sensitivity, the average mesh size, h, is defined to represent cell mesh size. Different rectangular meshes (h=1, 0.5, 0.25,...) are used to investigate the effect of mesh refinement. Simulations are performed to obtain velocity magnitude and temperature contours at critical Ra number and critical positions (half-width, half-height and diagonal lines). The mesh size of h=1 is selected as a coarse mesh and then in every refinement step it is divided by two as the finer mesh. Mesh sensitivity analysis is carried out in AR=2, $Ra = 1 \times 10^5$ and Pr=1 since these values are the most critical ones. The no-slip velocity boundary condition on walls results in zero velocity on walls. In addition, the velocity magnitude values are mostly constant for half-width line. Therefore, the half-height and diagonal lines of domain are selected to compare the velocity magnitude values.

Velocity magnitude at half-height and on diagonal line are plotted for different mesh sizes as shown in Figure 3.3 (a) and (b). By comparing the results, one can notice that the shape of velocity magnitudes are the same for different mesh sizes but the amplitude of them varies for the first three mesh sizes. There is no significant change in results when the mesh is refined further after h=0.25.

Although, the temperature values are not so sensitive to selected mesh sizes, the half-width and half-height positions are selected to represent the temperature contours for various mesh sizes. Results are plotted in Figure 3.4 (a) and (b). It can be seen that the temperature contours are not so sensitive to mesh size and for the mesh sizes finer than h=0.5, the temperature contours don't change.

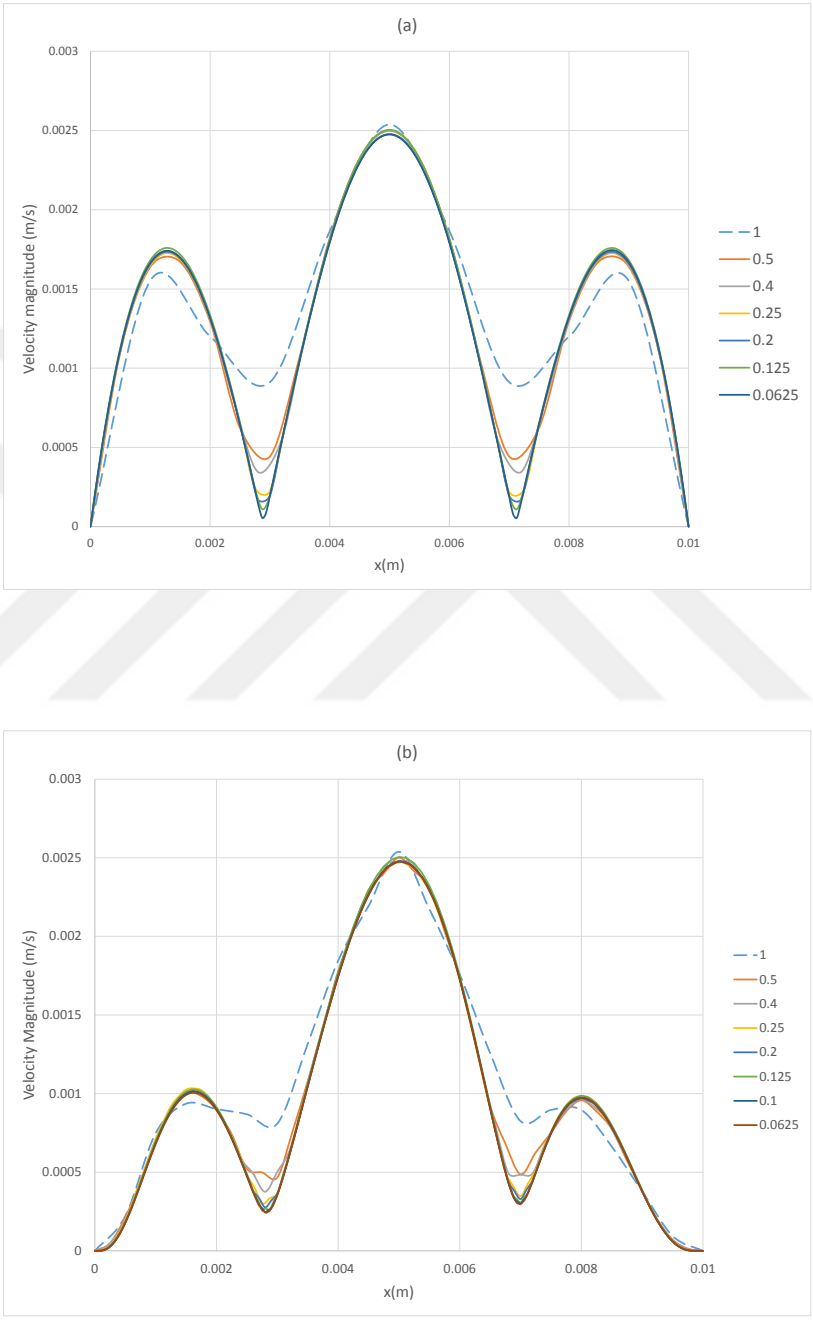

Figure 3.3. Velocity magnitude for AR=2, $Ra = 1 \times 10^5$ and Pr=1 for different mesh sizes; a) in x-direction at half-height; b) on the diagonal of the domain.

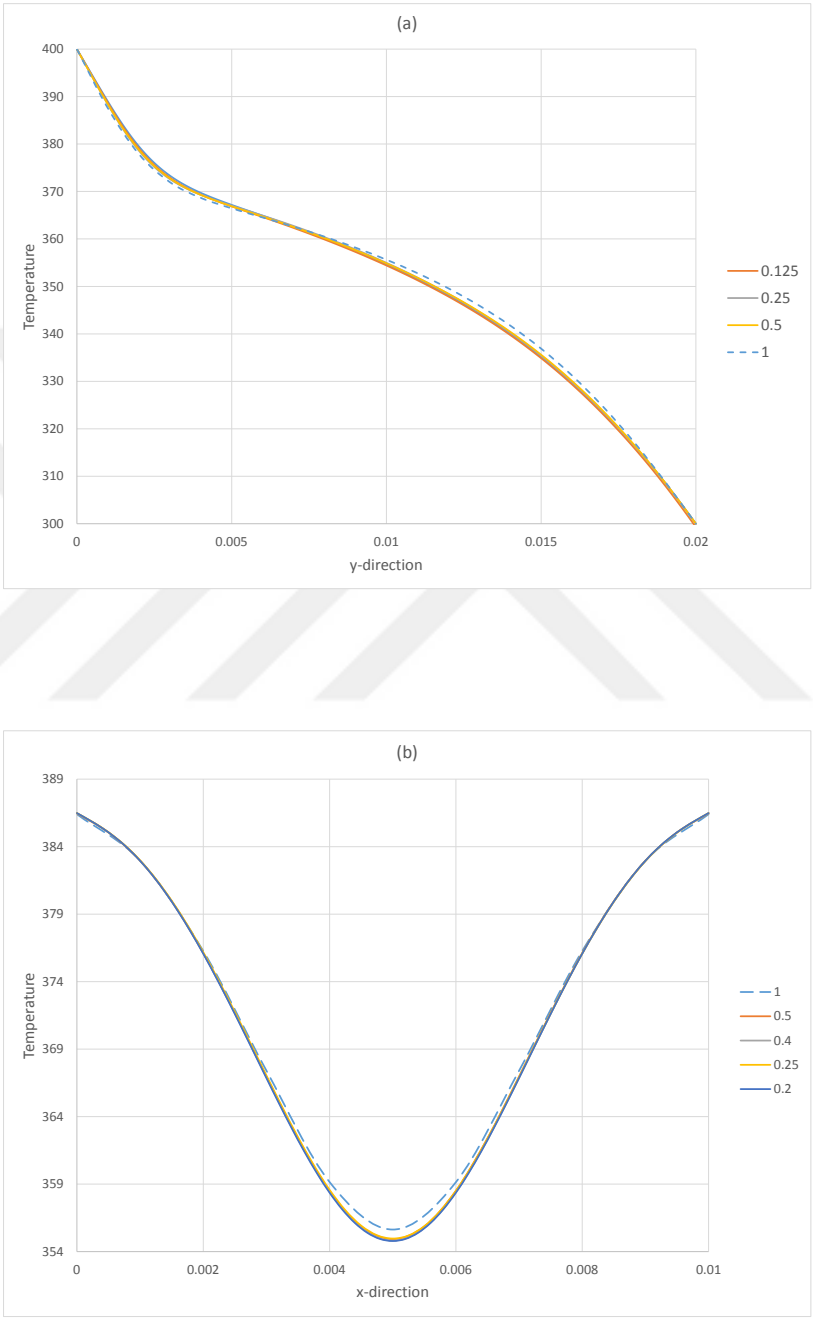

Figure 3.4. Temperature plots for AR=2, $Ra = 1 \times 10^5$ and Pr=1 for different mesh sizes; a) in y-direction at half-width; b) in x-direction at half-height.

3.4. Pseudo Transient Continuation

The pseudo transient method or pseudo-transient continuation is a practical technique of solving steady-state nonlinear differential equations [41]. In other words, it is a technique for solving the steady-state problem of time-evolving partial differential equations by setting an initial guess and using a time-stepper to evolve the solution forward. This algorithm effectively adds an unsteady term to the solution equations in order to improve stability and convergence behavior. Use of this option is recommended for general fluid flow problems. The technique is common to solve nonlinear equations when the initial iterate is far from a solution or can converge to nonphysical solutions or local minima of the norm of the steady-state residual. This is particularly the case when the solution has complex features, such as shocks or discontinuities, that are not present in the initial iterate. This method is useful in Transition Natural Convection i.e the Ra number is higher than critical Ra number.

The pseudo transient method is a form of implicit under-relaxation which is applied to the Equation 3.3. Here, the under-relaxation is controlled through the pseudo time step size. By using the pseudo transient under-relaxation, the linearized Equation 3.3 becomes:

$$\rho_P \Delta V \frac{\phi_P - \phi_P^{old}}{\Delta t} + a_P \phi_P = \sum_{nb} a_{nb} \phi_{nb} + b \tag{3.9}$$

where Δt is the pseudo time step. There are two kind of pseudo transient time step: automatic and fix. The automatic time step is calculated using the minimum of the different timescales:

$$\Delta t = Min(\Delta t_u, \Delta t_p, \Delta t_g) \tag{3.10}$$

Each time scale is obtained by dividing length scale L_{scale} over an appropriate velocity scale which depends on the physics present in the flow domain.

For solving the natural convection, the gravitational time scale Δt_g plays important role and is defined by the following equation:

$$\Delta t_g = \sqrt{\frac{L_{scale}}{g}} \tag{3.11}$$

where $g = |\vec{g}|$ is the magnitude of the gravitational vector, and for natural convection (the Boussinesq approximation) g is modified as follows:

$$g = |\vec{g}|\beta(T_{max} - T_{min}) \tag{3.12}$$

The convective time scale Δt_u is defined as:

$$\Delta t_u = \frac{0.3L_{scale}}{Max(U_{bc}, U_{domain})} \tag{3.13}$$

The velocity U_{bc} is the maximum of the arithmetic average of the velocity at the domain boundary faces, and U_{domain} is the arithmetic average of the velocity over the cells in the domain. The dynamic time scale Δt_p is defined as:

$$\Delta t_p = \frac{0.3L_{scale}}{U_{\Delta P}} \tag{3.14}$$

The velocity scale $U_{\Delta P}$ is based on the pressure difference at open boundaries, such as pressure inlet, pressure outlet or velocity inlet, and is defined by the following:

$$U_{\Delta P} = \sqrt{(\frac{P_{bc,max} - P_{bc,min}}{\bar{\rho}_{cells}})} \tag{3.15}$$

where $P_{bc,max}$ is the maximum pressure value at the open boundary. $P_{bc,min}$ is the minimum pressure value at the open boundary, and $\bar{\rho}_{cells}$ is the average density over the domain.

To represent this, the length scale L_{scale} should be defined. Two length scale calculation methods are available: aggressive and conservative. If the aggressive length scale method is applied, then the length scale in all of the equations shown above are defined as:

$$L_{scale} = MAX(L_{vol}, L_{ext}) \tag{3.16}$$

On the other hand, if the conservative length scale method is applied, then the length scale is defined as

$$L_{scale} = MIN(L_{vol}, L_{ext}) \tag{3.17}$$

where the volume length scale is defined as:

$$L_{vol} = \sqrt[3]{V} \tag{3.18}$$

and the domain length scale is defined as

$$L_{ext} = MAX(L_x, L_y, L_z) \tag{3.19}$$

where V is the volume of the domain and (L_x, L_y, L_z) are the domain lengths in the x,y,z direction.

3.4.1. Application of pseudo transient continuation at critical Ra number regions

Pseudo transient continuation helps the convergence, and stabilize unstable or periodic residuals. Here, the utilization of SIMPLE scheme and Coupled scheme with using pseudo-transient method is compared. At critical or high Ra numbers, the Pseudo-transient method is very helpful to converge gradually the momentum and energy equations. Given that in unstable and critical Ra number region the convergence of momentum and energy equation is difficult, this method is useful to help them converge gradually. The Pseudo transient continuation is used to help convergence for both divergence in residuals and periodic residuals as shown in Figures 3.5 (a) and 3.6 (a), respectively.

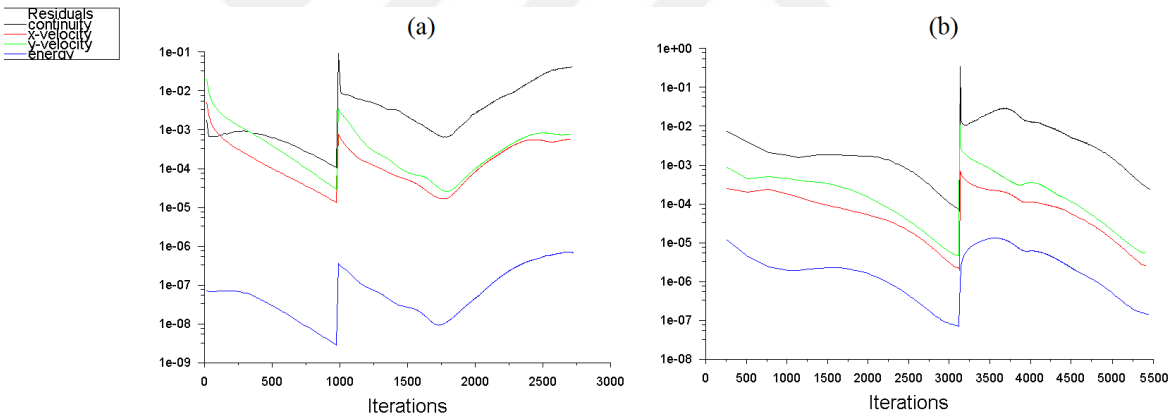

Figure 3.5. Residual-iteration plot at $Ra = 2 \times 10^5$ and Pr=0.5; a) utilizing SIMPLE scheme for pressure-velocity coupling; b) using Coupled scheme for pressure-velocity coupling with Pseudo transient.

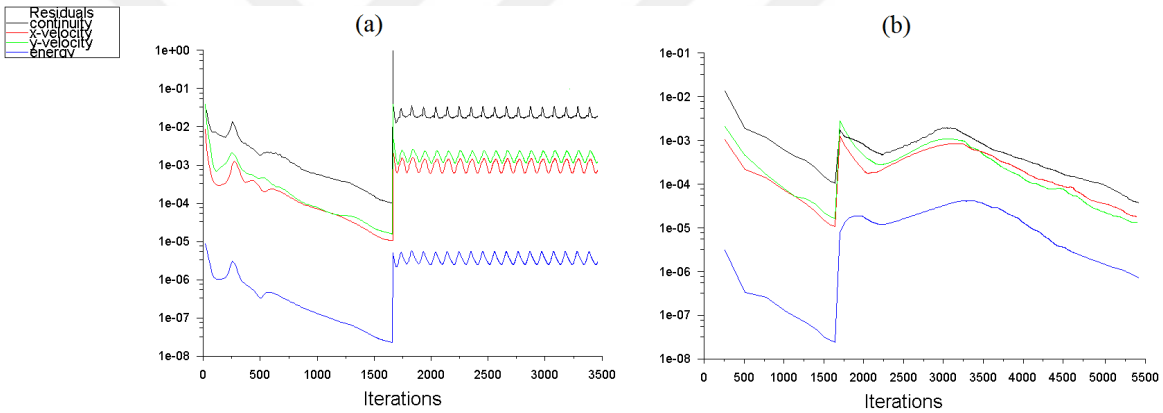

Figure 3.6. Residual-iteration plot at $Ra = 1 \times 10^6$, Pr=5; a) utilizing SIMPLE scheme for pressure-velocity coupling; b) using Coupled scheme for pressure-velocity coupling with Pseudo transient.

3.5. Monitoring Residuals

At the end of each solver iteration, the residual sum for each of the conserved variables is computed and stored, thus recording the convergence history. This history is also saved in the data file. On a computer with infinite precision, these residuals will go to zero as the solution converges. On an actual computer, the residuals decay to some small value ("round-off") and then stop changing ("level out"). For single-precision computations (the default for workstations and most computers), residuals can drop as many as six orders of magnitude before hitting round-off. Double-precision residuals can drop up to twelve orders of magnitude. Guidelines for judging convergence can be found in Judging Convergence section.

3.5.1. Definition of Residuals

The conservation equation for a general variable ϕ at a cell P is linearized in Equation 3.3 . The residual R^{ϕ} in Equation 3.3 is summed over all the computational cells P. This is referred to as the "unscaled" residual.

$$R^{\phi} = \sum_{cellsP} |\sum_{nb} a_{nb}\phi_{nb} + b - a_P\phi_P| \tag{3.20}$$

In general, it is difficult to judge convergence by examining the residuals defined by Equation 3.20 since no scaling is employed. This is especially true in enclosed domains such as natural convection where there is no inlet flow rate of ϕ to compare the residual. There are two kinds of scaling factors to scale the residuals. The factors are termed *global scaling* and *local scaling*. The "globally scaled" residual is defined as

$$R^{\phi} = \frac{\sum_{cellsP} |\sum_{nb} a_{nb}\phi_{nb} + b - a_P\phi_P|}{\sum_{cellsP} |a_P\phi_P|} \tag{3.21}$$

The "locally scaled" residual is defined as

$$R^{\phi} = \frac{\sqrt{\sum_{cells P}^{n} (\frac{1}{n})(\frac{\sum_{nb} a_{nb}\phi_{nb} + b - a_P\phi_P}{a_P})^2}}{(\phi_{max} - \phi_{min})_{domain}} \tag{3.22}$$

For both residual scale in momentum equation the ϕ is replaced by velocity magnitude at the cell P.

3.5.2. Judging Convergence

There are no universal metrics for judging convergence. Residual definitions that are useful for one class of problem are sometimes misleading for other classes of problems. Some convergence criterion is defined for most problems. This criterion requires that the globally scaled residuals, defined by Equation 3.21 decrease to 10^{-3} for all equations except the energy, for which the criterion is 10^{-6} . Locally scaled residuals defined by Equation 3.22 decrease to 10^{-5} for all equations. Sometimes, however, this criterion may not be appropriate. Typical situations are listed below.

- In cases with a good initial guess of the flow field, the initial continuity residual may be converged quickly leading to a large scaled residual for the continuity equation. In such situations, it is useful to examine the unscaled residual for continuity equation.
- In non-linear problems such as natural convection, is used for continuity and momentum equations with a poor initial guess result in divergence (high scale factors). In such cases, scaled residuals will start to diverge, increase as non-linear sources build up, and eventually decrease. The first convergence is due to a local minima and therefore it is not the right results for the problem. Hence, setting the scaled residual to 10^{-5} and increasing the number of iterations, ensures that the residual continues to decrease (or remain low) before concluding that the solution has converged.

In this thesis, for convergence criterion, the global scaled residual is used with 10^{-5} for continuity and momentum equations, and 10^{-8} for energy equation. In Figures 3.7, 3.8, and 3.9 , the converged residuals are shown for a range of Ra number with constant AR and Pr. The Ra continuation is used in these figures.

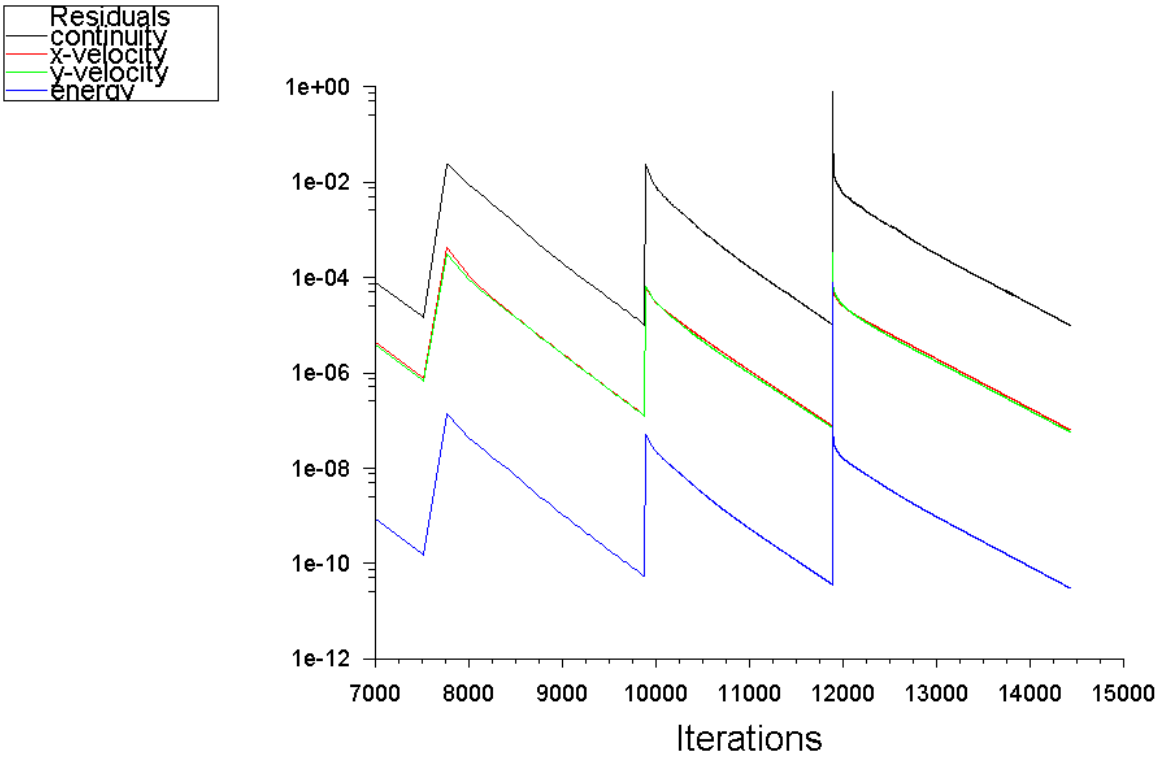

Figure 3.7. Residuals for constant AR=1/2, Pr=5; Ra continuation from $Ra = 2000$ to $Ra = 5 \times 10^4$ and boundary condition continuation from BC1 to BCI (insulated boundary condition on side walls).

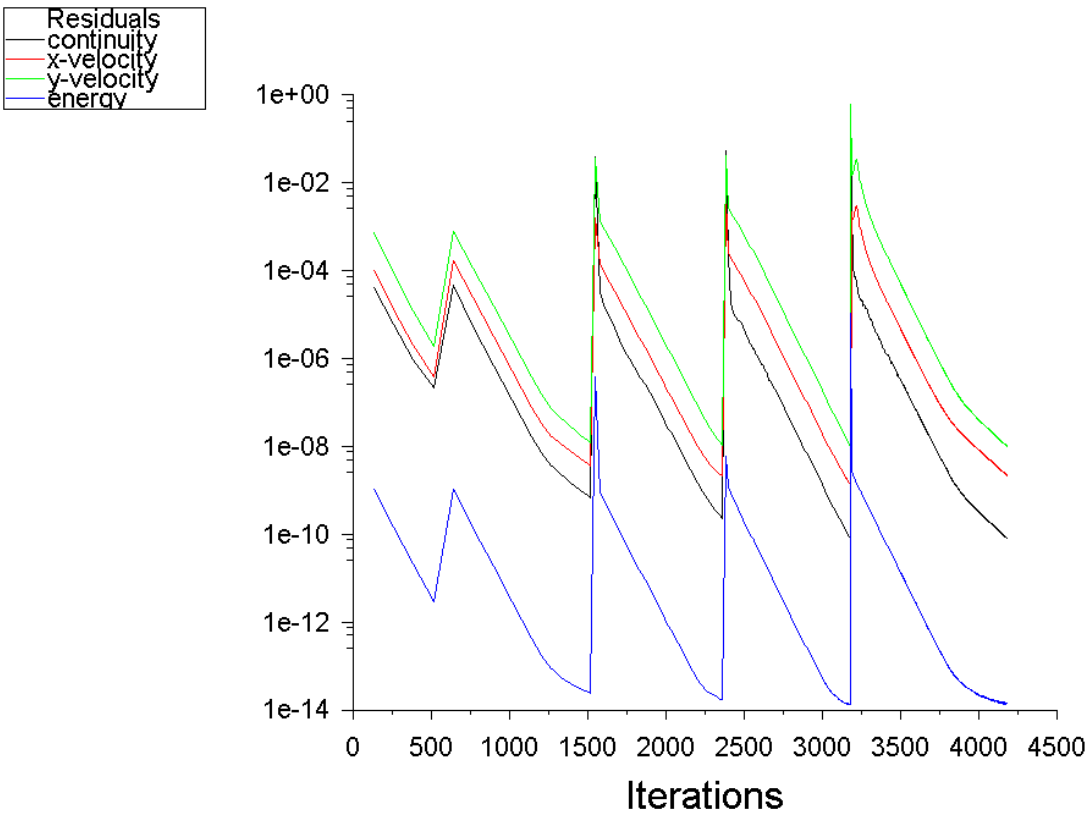

Figure 3.8. Residuals for constant AR=4, Pr=1; Ra number continuation from $Ra = 1 \times 10^4$ to $Ra = 8 \times 10^4$ and boundary condition continuation from BC1 to BCI (insulated boundary condition on side walls).

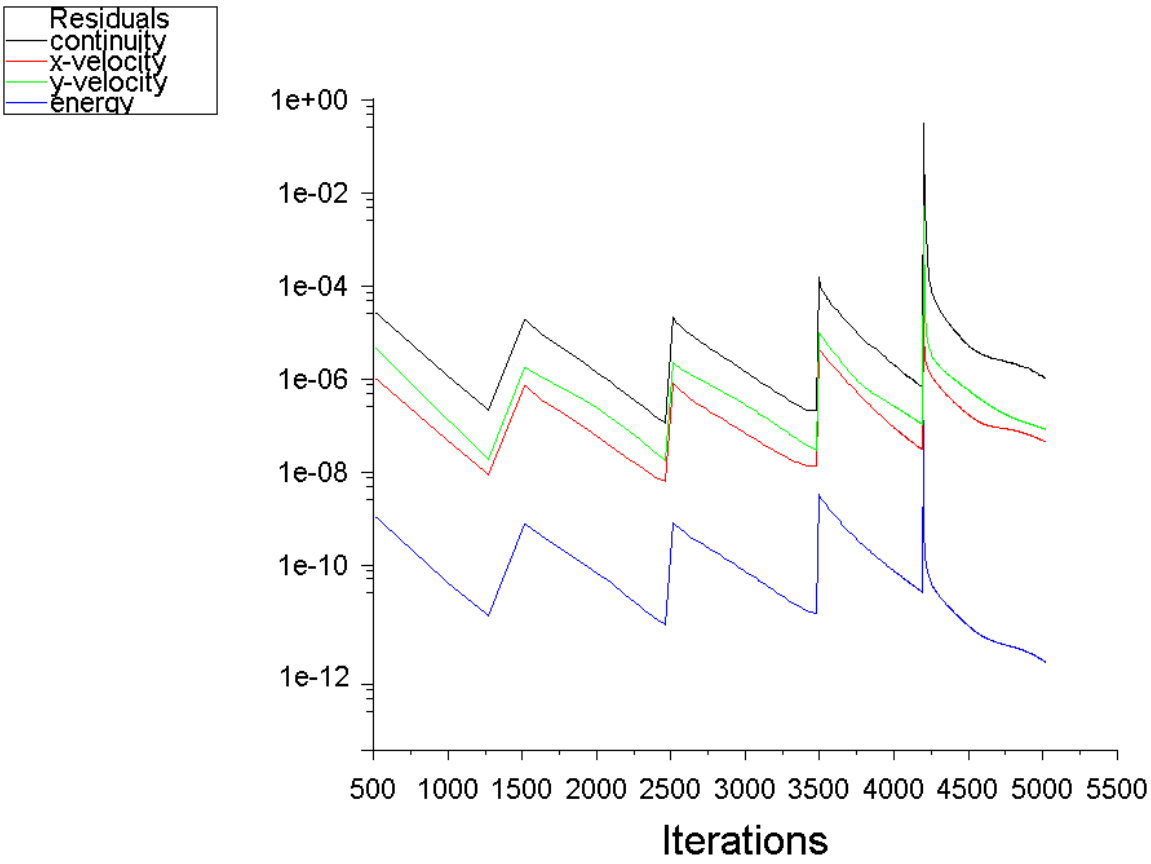

Figure 3.9. Residuals for constant $Ra = 2 \times 10^5$, Pr=0.5, and AR=2; Ra number continuation from $Ra = 5 \times 10^4$ to $Ra = 2 \times 10^5$ and boundary condition continuation from BC1 to BCI (insulated boundary condition on side walls).

4. RESULTS AND DISCUSSIONS

In this part, the results of transition and multiplicity phenomena on different cases are represented. A combination of thermal and hydrodynamic effects yield complex multiple flow patterns. First part of the results is devoted to the parametric investigation of Rayleigh-Benard Instability. The effects of Ra, Pr and BC are investigated in this part by varying one parameter and keeping the others constant. Second part of the results is devoted to show the transition natural convection for different AR. The continuation methods play fundamental role to follow the result path to show the transition phenomenon in this part. Finally, multiplicity phenomenon for different ARs is shown and compared with literatures. The BC continuation method helps to obtain multiple convective patterns in fix parameters. Indeed, the BC and Ra continuation methods support to follow the various path of flow patterns after bifurcation points. The Ra continuation is a useful method to find critical Ra numbers and bifurcation points. At critical or high Ra numbers which the convergence of equation is not satisfied, a pseudo-transient method is used where time is an iteration parameter until the solution is obtained.

4.1. Rayleigh Benard Instability

In this section, a parametric analyse for various Ra, Pr and AR is carried out. In every case, the BC continuation method is utilized on vertical walls. In this study, the boundary condition of Rayleigh-Benard problem is applied to all cases as shown in Figure 2.1. The Rayleigh-Benard instability develops when Ra number is above a critical value. The rectangular cavity has been studied for different ARs (1/4, 1/2, 2, and 4). Different Ra number effects is examined for constant AR=1/2 and Pr=5. The velocity magnitude and Nu number are shown in Table 4.1 for six cases with Ra numbers between 2000 and 1×10^6.

Rayleigh	Velocity magnitude	Nusselt
2000	4.28×10^{-8}	0.4
5000	2.1×10^{-4}	2.59
1×10^{4}	4.02×10^{-4}	7.63
1×10^{5}	3.5×10^{-3}	15.37
5×10^{5}	4.27×10^{-3}	17.01
1×10^{6}	8.5×10^{-3}	21.25

Table 4.1. Parametric analysis at different Ra numbers for constant $AR = 1/2$ and $Pr = 5$.

The results show that by increasing the Ra number, velocity magnitude and Nu number increase in a non-linear manner as shown in Figure 4.1. The increase in both velocity and Nu can be described in three stages: at the first stage ($2000 < Ra < 1 \times 10^5$), it increases drastically; the second stage ($1 \times 10^5 < Ra < 5 \times 10^5$) is more like a plateau at which the increase in the velocity or Nu is negligible compared to the increase in Ra; at the third stage ($5 \times 10^5 < Ra < 1 \times 10^6$) , the curve starts to increase but the slope is smaller compared to the slope of the first stage. The second stage is indeed the transition region from two symmetric velocity cells to four symmetric velocity cells.

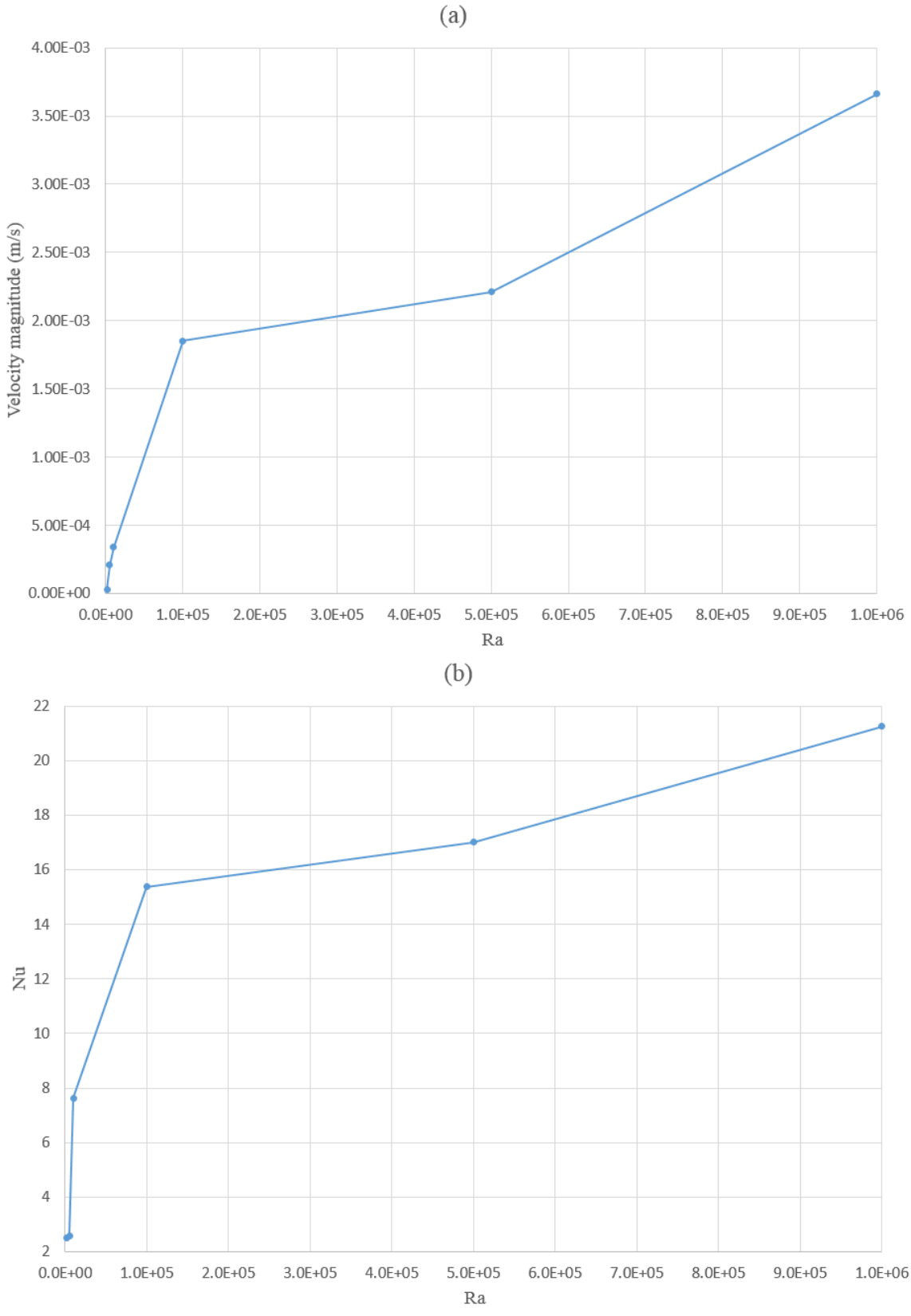

Figure 4.1. Plots showing the variation of velocity magnitude and Nu number with respect to Ra numbers for constant $AR = 1/2$ and Pr=5; a) Ra-velocity magnitude; b) Ra-Nu.

The velocity magnitude vectors and temperature contours for different Ra numbers are shown in Figures 4.2 and 4.3. In fact, the transition phenomenon for AR=1/2 is depicted in these figures. By increasing the Ra number, convective flow within the domain is altered from two symmetric cells to four symmetric cells.

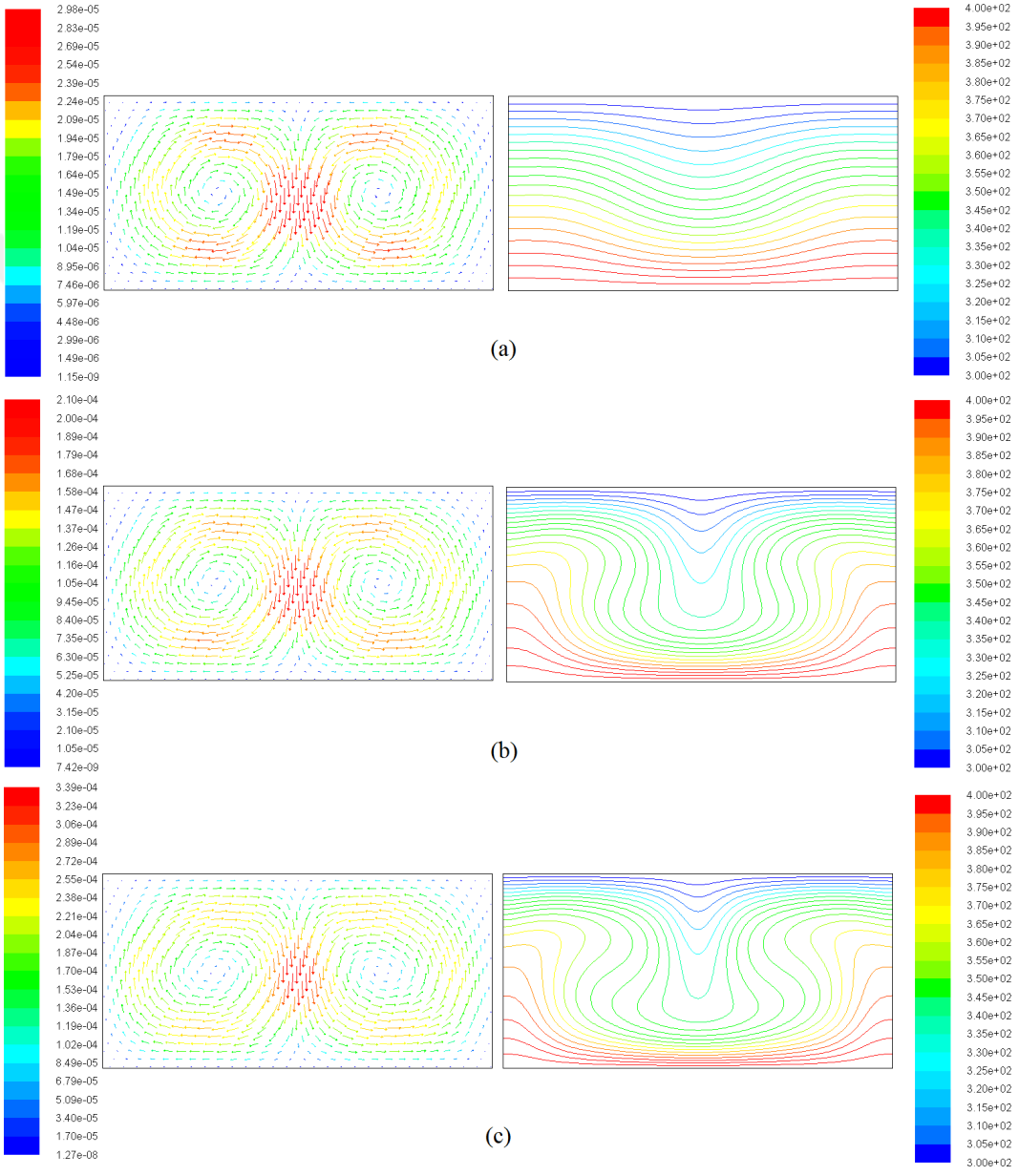

Figure 4.2. Temperature contours (right) and velocity magnitude vectors (left) for AR=1/2, Pr=5; a) Ra=2000; b) Ra=5000; c) $Ra = 1 \times 10^4$.

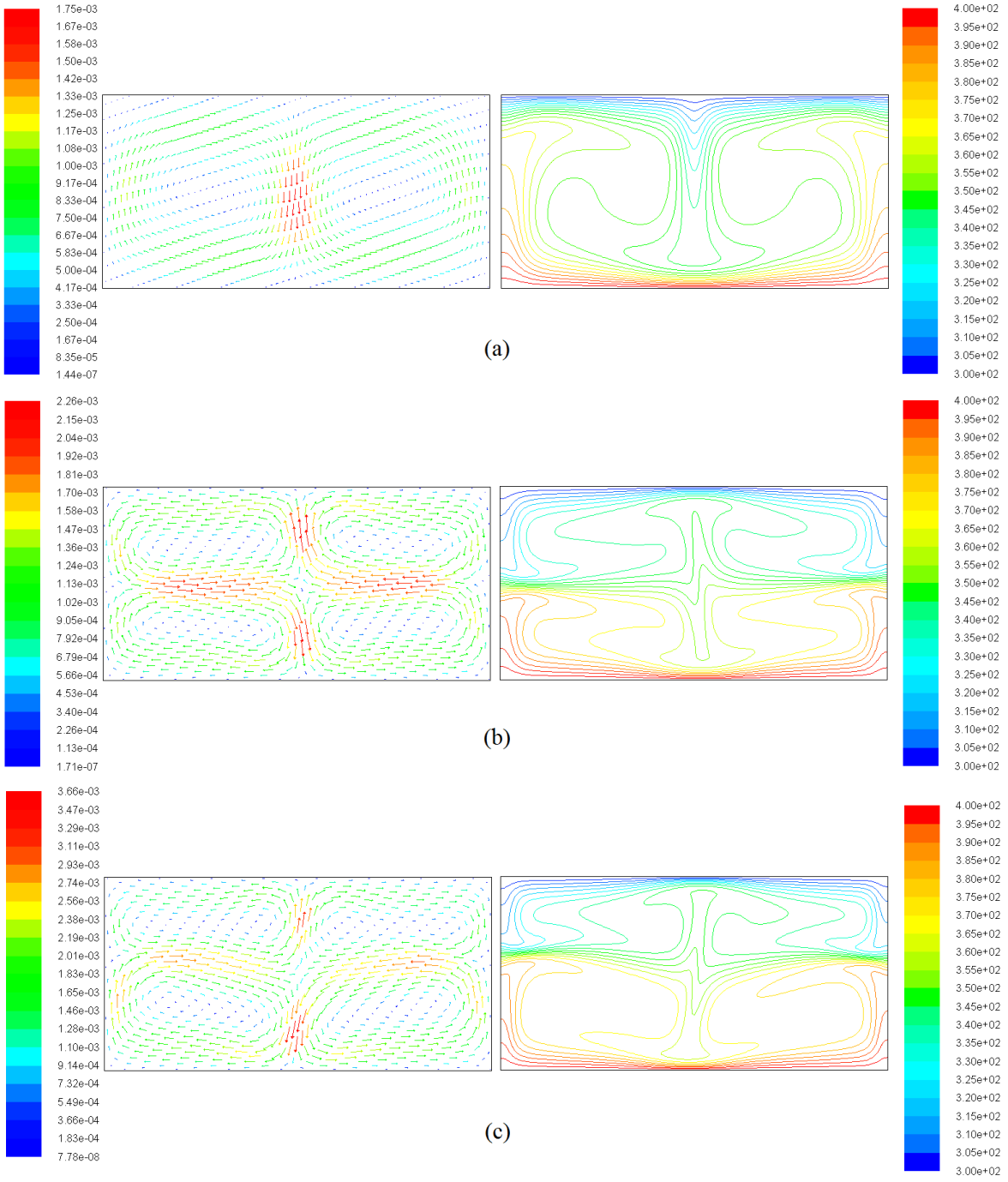

Figure 4.3. Temperature contours (right) and velocity magnitude vectors (left) for AR=1/2, Pr=5; a) $Ra = 1 \times 10^5$; b) $Ra = 5 \times 10^5$; c) $Ra = 1 \times 10^6$.

Five cases with AR=2 and Pr number between 0.1 and 10 were investigated as shown in Table 4.2. For all cases, the Nu number is bigger than 1 and heat transfer occurs by convection. By decreasing the Pr number from 10 to 0.1, the velocity magnitude is increased except for Pr=0.5 in which the magnitude of two kidney shape velocity cells is divided to four velocity cells that leads to a decrease in the velocity magnitude. At Pr=0.1, the velocity magnitude increases again. It can also be concluded that the critical Ra number increases with decreasing Pr number. Hence, at Pr=0.1 and Pr=0.5, four symmetric velocity cell exist (Figure 4.5). Indeed, the bifurcation point for transition from two-rolls to four-rolls for low Pr numbers(lower than one) occurs at low Ra number values in these cases as shown in Figure 4.5.

Pr	Velocity magnitude	Nusselt
0.1	0.00222	2.23
0.5	0.00176	3.43
1	0.00325	8.07
5	0.000835	12.647
10	0.000418	12.665

Table 4.2. Parametric analysis for a range of Pr numbers between 0.1 and 10 at constant $Ra = 2 \times 10^5$ and $AR = 2$; maximum value of the Nu number and velocity magnitude is obtained for each case.

The velocity magnitude is decreased except for Pr=0.5 in which the transition from two-rolls to four-rolls happens. In Figure 4.6, two kidney shape convective cells are observed for Pr numbers above the unity. The velocity magnitude decreased in this figure although the Pr number increased. The critical Ra number results in this observation. The higher velocity values are obtained for the cases which are in critical Ra number region.

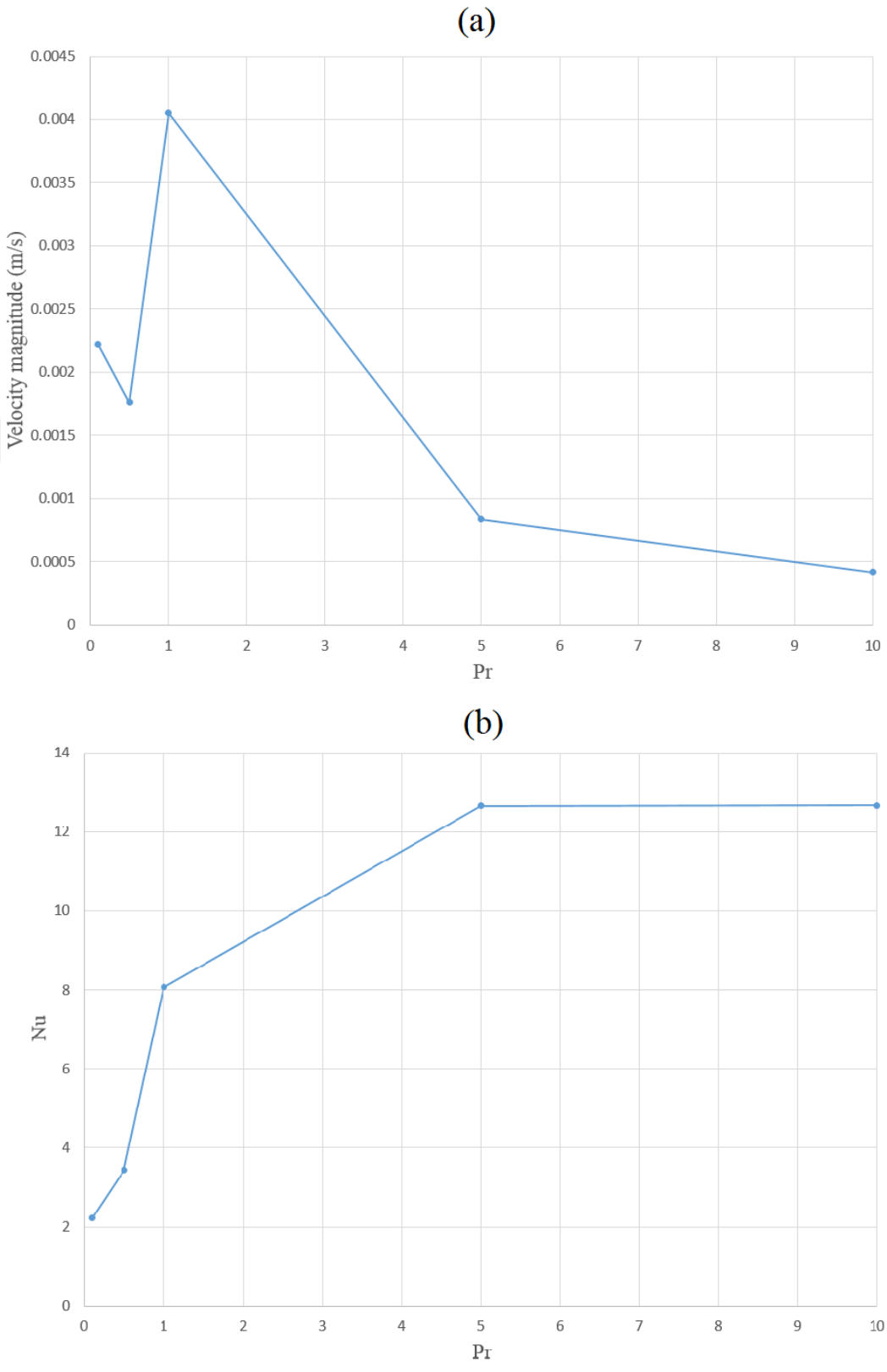

Figure 4.4. Plots showing the variation of velocity magnitude and Nu number with respect to constant Ra number and AR ($Ra = 2 \times 10^5$ and $AR = 2$); a) Pr-velocity magnitude; b) Pr-Nu.

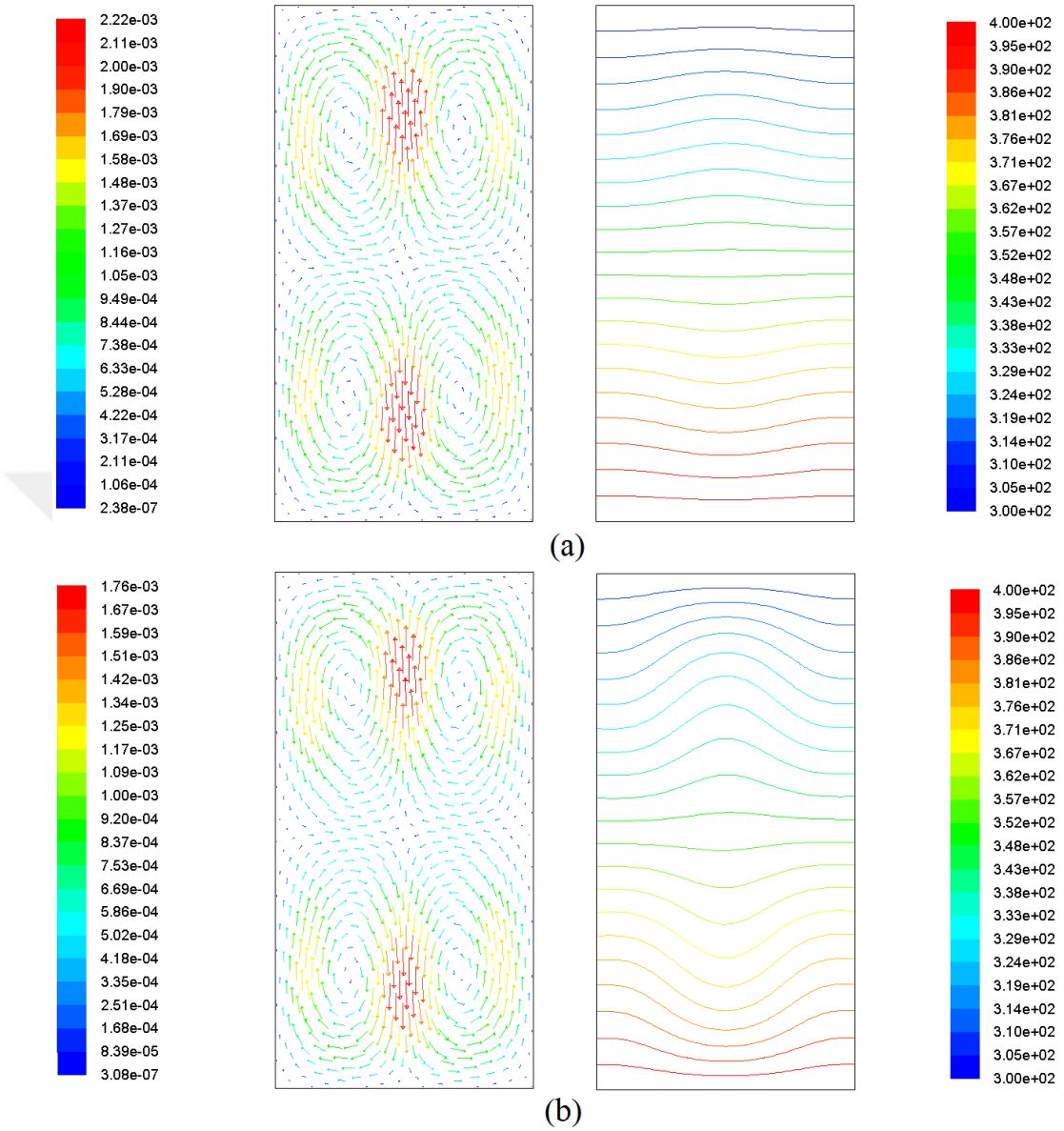

Figure 4.5. Temperature contours (right) and velocity vectors (left) at constant $Ra = 2 \times 10^5 and AR = 2$; a) Pr=0.1; b) Pr=0.5.

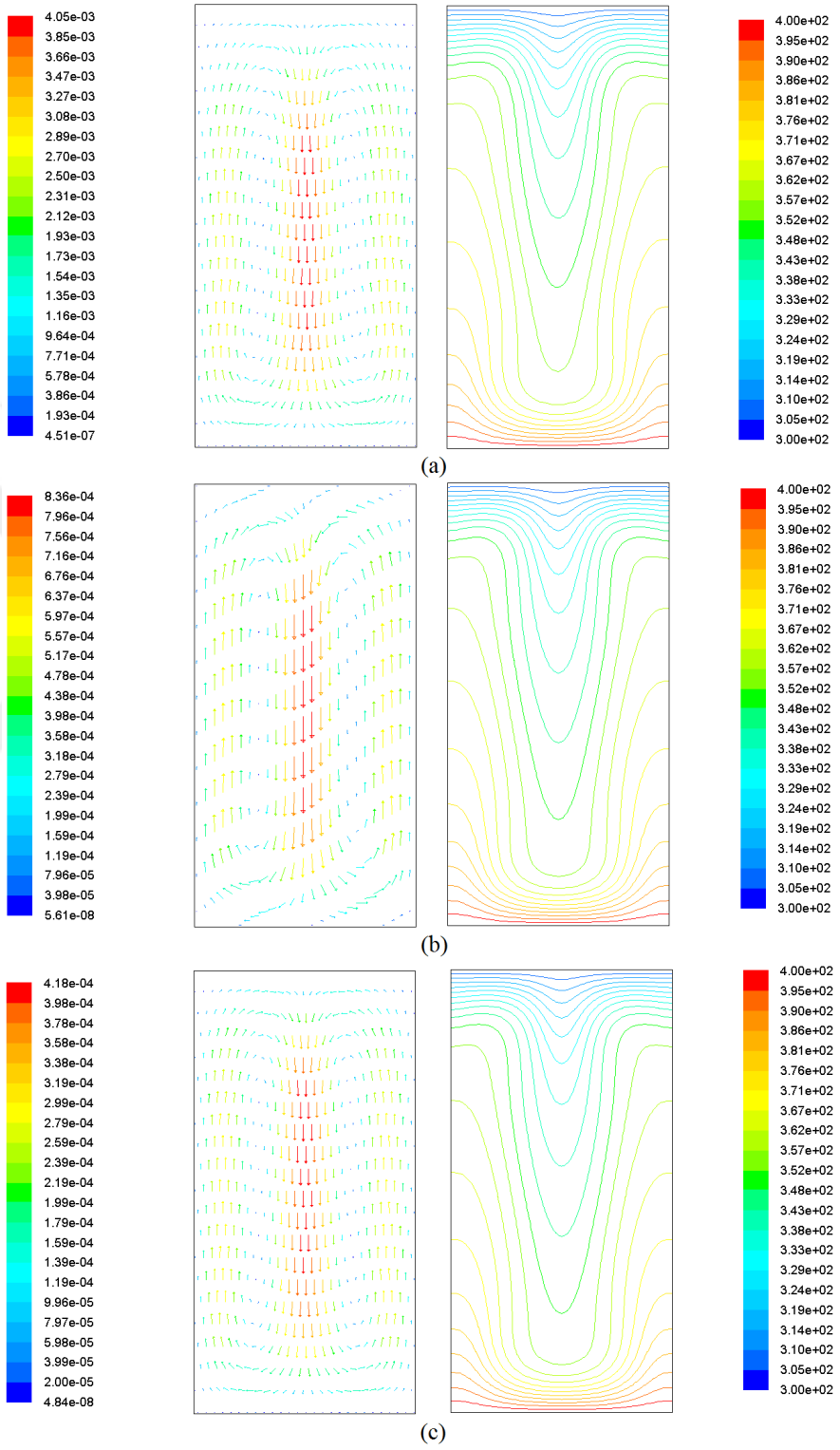

Figure 4.6. Temperature contours (right) and velocity vectors (left) at constant $Ra = 2 \times 10^5 and AR = 2$; a) Pr=1; b) Pr=5 ; c) Pr=10.

Table 4.3 shows the results for velocity magnitude and Nu number at $Ra = 8 \times 10^4$ and Pr=1 with ARs varying from 1/4 to 4.

AR	Velocity magnitude	Nusselt
1/4	0.0068	17.29
1/2	0.0065	16.08
1	0.00297	9.27
2	0.00118	3.93
4	0.00001	2

Table 4.3. Parametric analysis for different aspect ratio at constant $Ra = 8 \times 10^4$ and Pr=1 ; maximum value of the Nu number and velocity magnitude is obtained for each case.

Figure 4.7 shows the change in velocity and Nu for different ARs. One can see that both velocity and Nu have a reverse relation with respect to AR i.e. increasing the AR results in decreasing both parameters.

For AR=1/4, four symmetric convective cells are observed at $Ra = 8 \times 10^4$ as shown in Figure 4.8. The results are stable for cases with AR=1/2 and 1/4 (Figure 4.8 (a) and (b)). The transition from two-cells to four-cells patterns occurs in AR=1 as shown in Figure 4.8 (c). This is explained in details in Section 4.3. It should be noted that the critical Ra number occurs in higher ordes (10^5 and 10^6) for AR=2 and 4. Hence, two stable kidney shape cells are observed for these cases as shown in Figure 4.9 and 4.10. Comparing Figures 4.8, 4.9 and 4.10, it can be interpreted that the critical Ra number increases with decreasing AR.

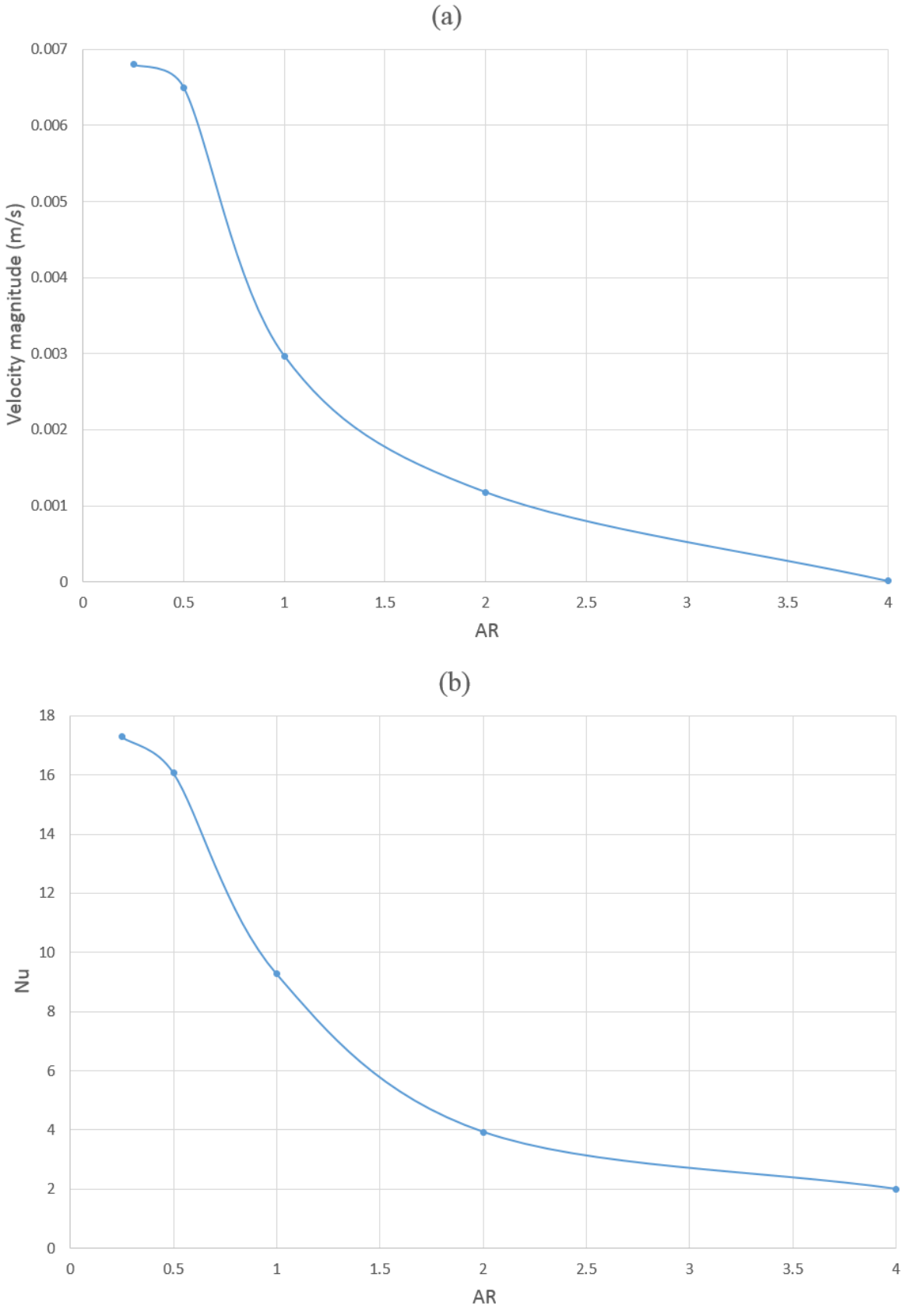

Figure 4.7. Plots showing the variation of velocity magnitude and Nu number with respect to constant Ra and Pr numbers ($Ra = 8 \times 10^4$ and $Pr = 1$); AR-velocity magnitude; b) AR-Nu.

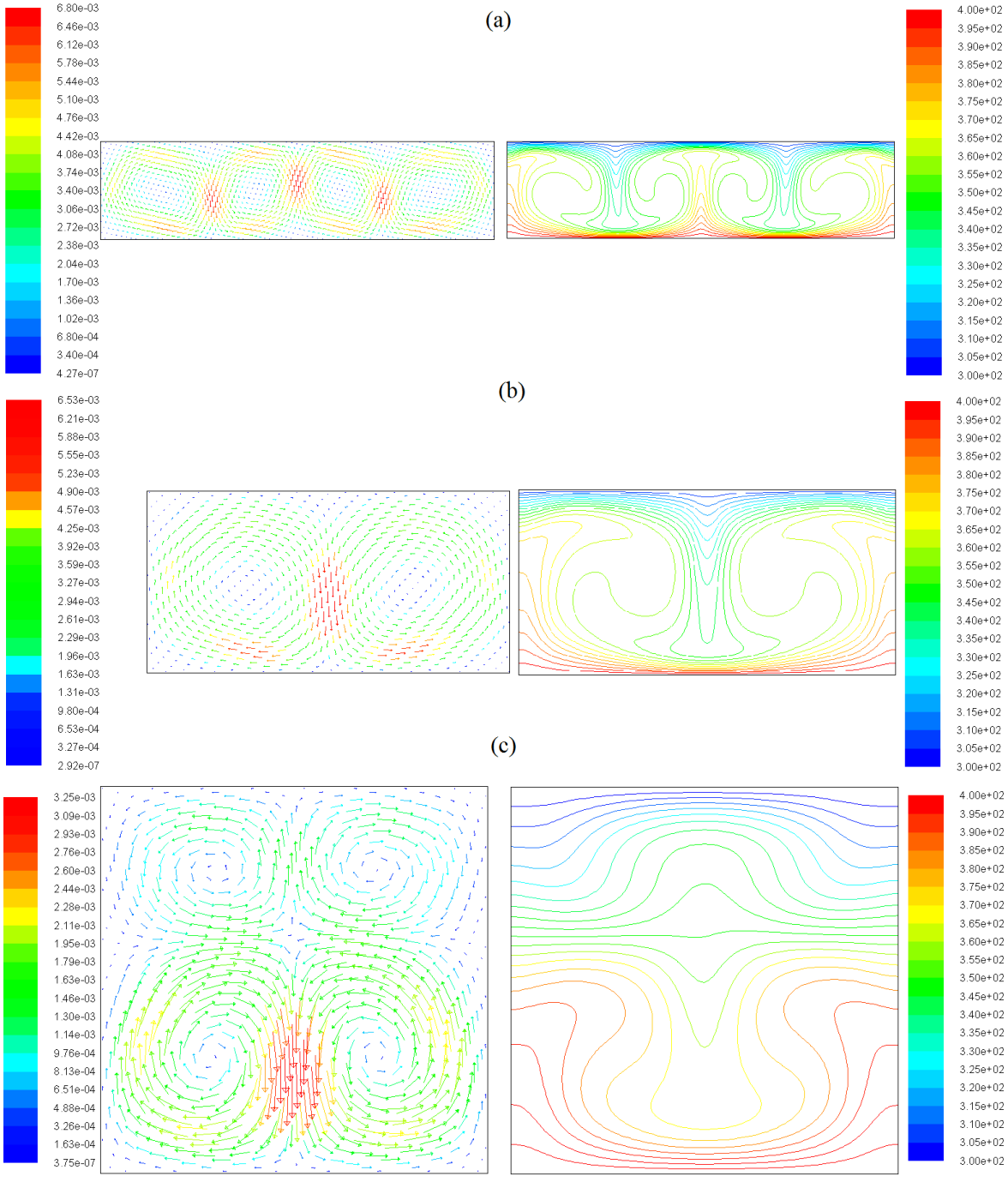

Figure 4.8. Temperature contours (right) and velocity vectors (left) at constant $Ra = 8 \times 10^4$ and Pr=1; a) AR=1/4; b) AR=1/2 ; c) AR=1.

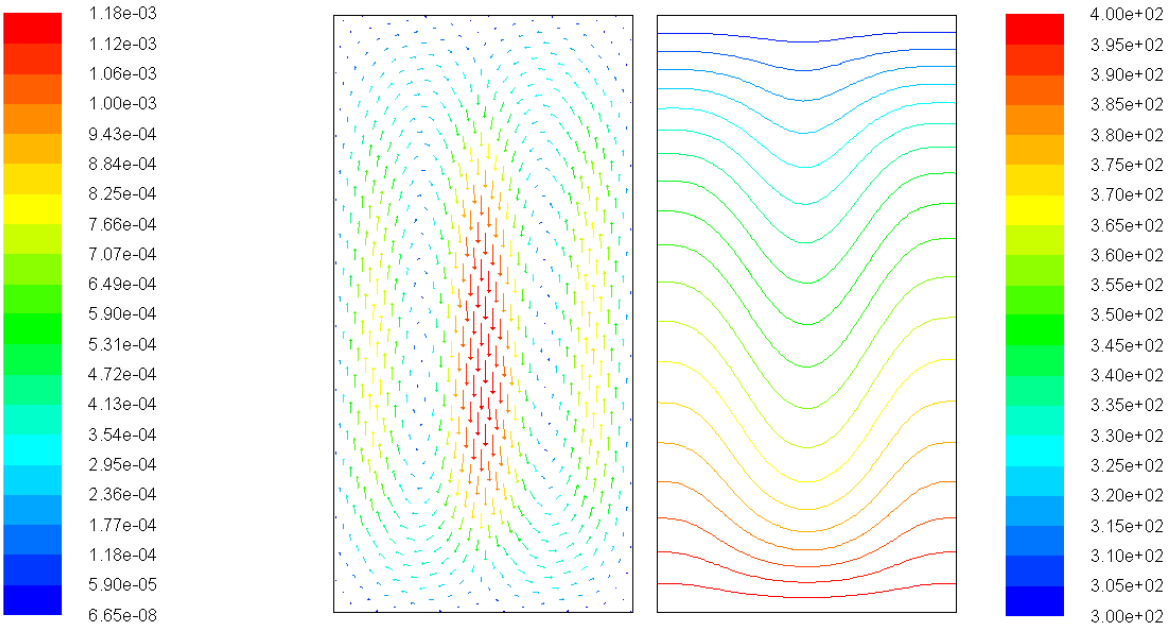

Figure 4.9. Temperature contours (right) and velocity vectors (left) at constant $Ra = 8 \times 10^4$ and Pr=1, and AR=2.

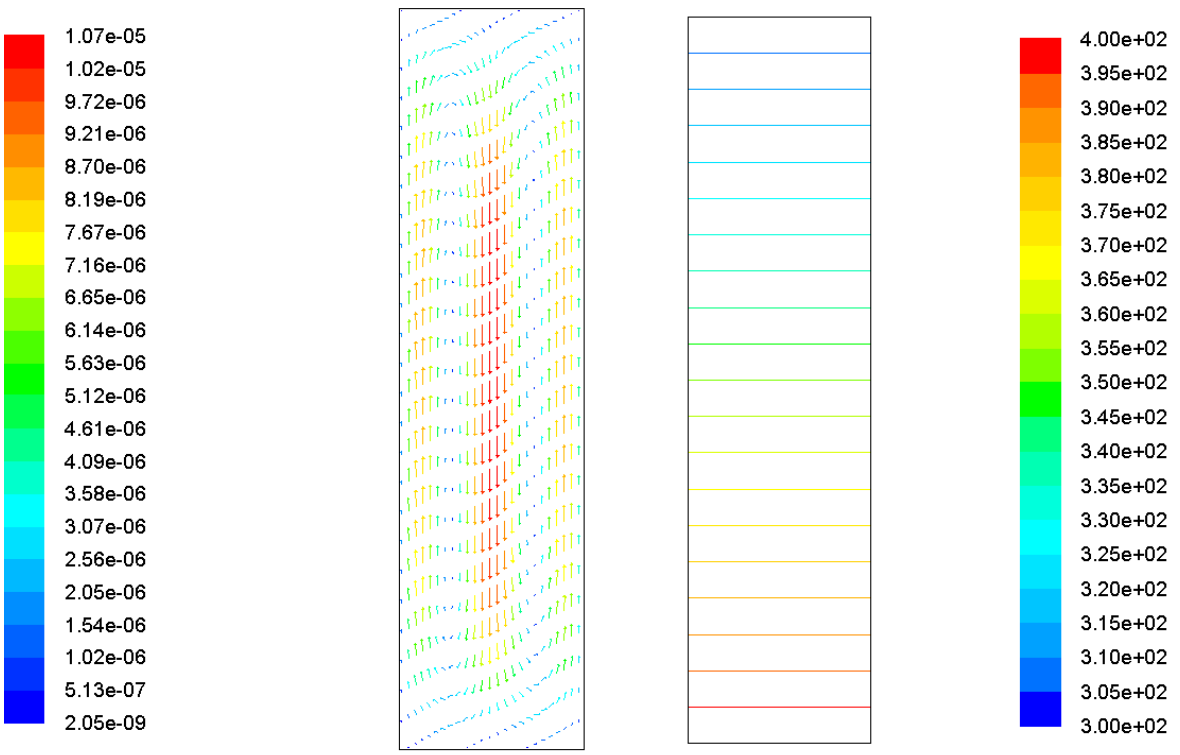

Figure 4.10. Temperature contours (right) and velocity vectors (left) at constant $Ra = 8 \times 10^4$ and Pr=1, and AR=4.

4.2. Transition phenomenon

The convective flow for high Pr number forms two symmetric kidney-shaped or crescent-shaped cells in which fluid rises and sinks in different flow patterns. Higher order temperature gradients (Figure 4.11) are used on walls as an initial values to investigate the transition and multiplicity phenomenon for different ARs. The bottom (hotter) wall set to 400°k and top wall temperature is 300°k. The linear BC is called BCL, and the BCs with odd numbers (BC1, 3, 5, ..) are above BCL, and the even numbers are below it (BC2, 4, 6). The final Rayleigh-Benard BC is used for all cases which is an insulated BC (BCI).

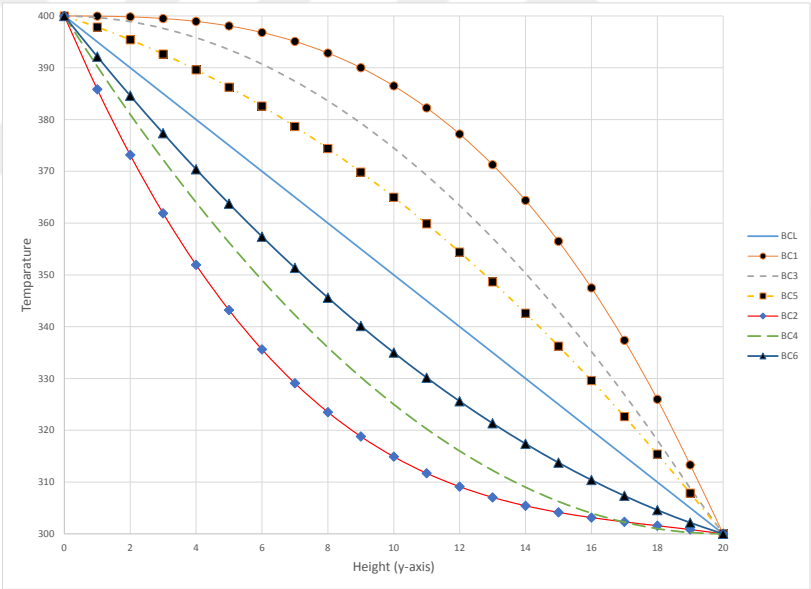

Figure 4.11. Higher order temperature boundary conditions on walls.

For the first observation of transition phenomenon the AR=1 is selected in Figure 4.12. In this case (Pr=1), the critical Ra (for bifurcation from 2-cells to 4-cells) is happened within the range of $4 \times 10^4 - 5 \times 10^4$. However, the multiple results are observed for this case at low Ra number by using BC continuation (Figure 4.15), at higher Ra number (bigger than critical Ra) the direction of velocity cells are the

same. In four-rolls pattern results, the pair of cells at the bottom are always sink down from the middle of domain. It shows that at the bottom half of domain, the gravity force imposes bouncy force. In Figure 4.12 (top), convective flow is stable at $Ra = 3 \times 10^4$ and two symmetric kidney-shaped cell is obtained. At $Ra = 6 \times 10^4$ two cells appears at the bottom Figure 4.12 (in second row, the first one from left).Then by using the Ra continuation, transition to four symmetric cells is obtained at $Ra = 7 \times 10^4$, $Ra = 8 \times 10^4$. In Figure 4.13, the transition results are shown for $Ra = 5 \times 10^5$, AR=2, and Pr=1. Here, the various BC initial values change the shape of convective flow patterns.

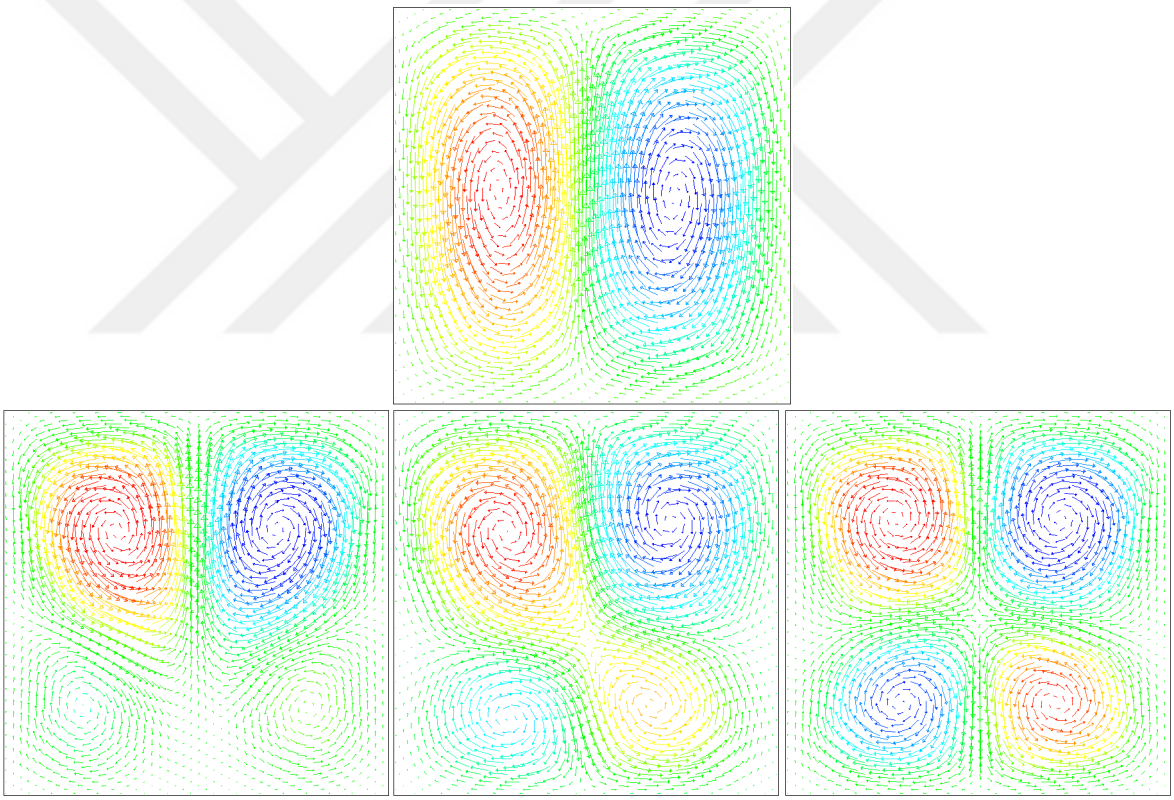

Figure 4.12. Transition results by using Ra and BC continuation methods.

Transition of convective flow from four symmetric cells to six-rolls is shown in Figure 4.14 . The results show that the flow patterns are separated from the middle of domain by two small cells.

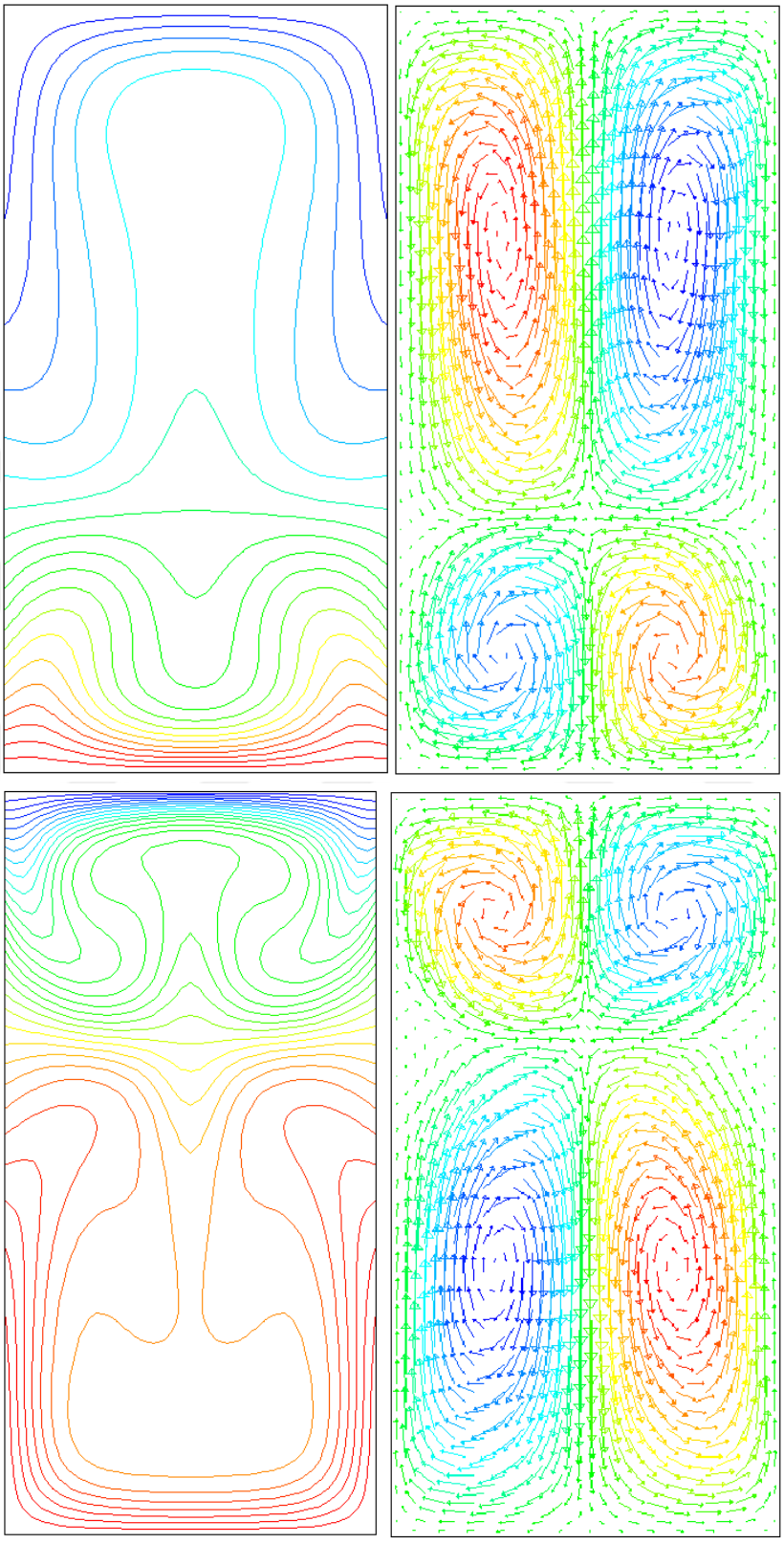

Figure 4.13. Transition results $Ra = 5 \times 10^5$, AR=2, and Pr=1; by using odd number BCs (top) and even number BCs (bottom).

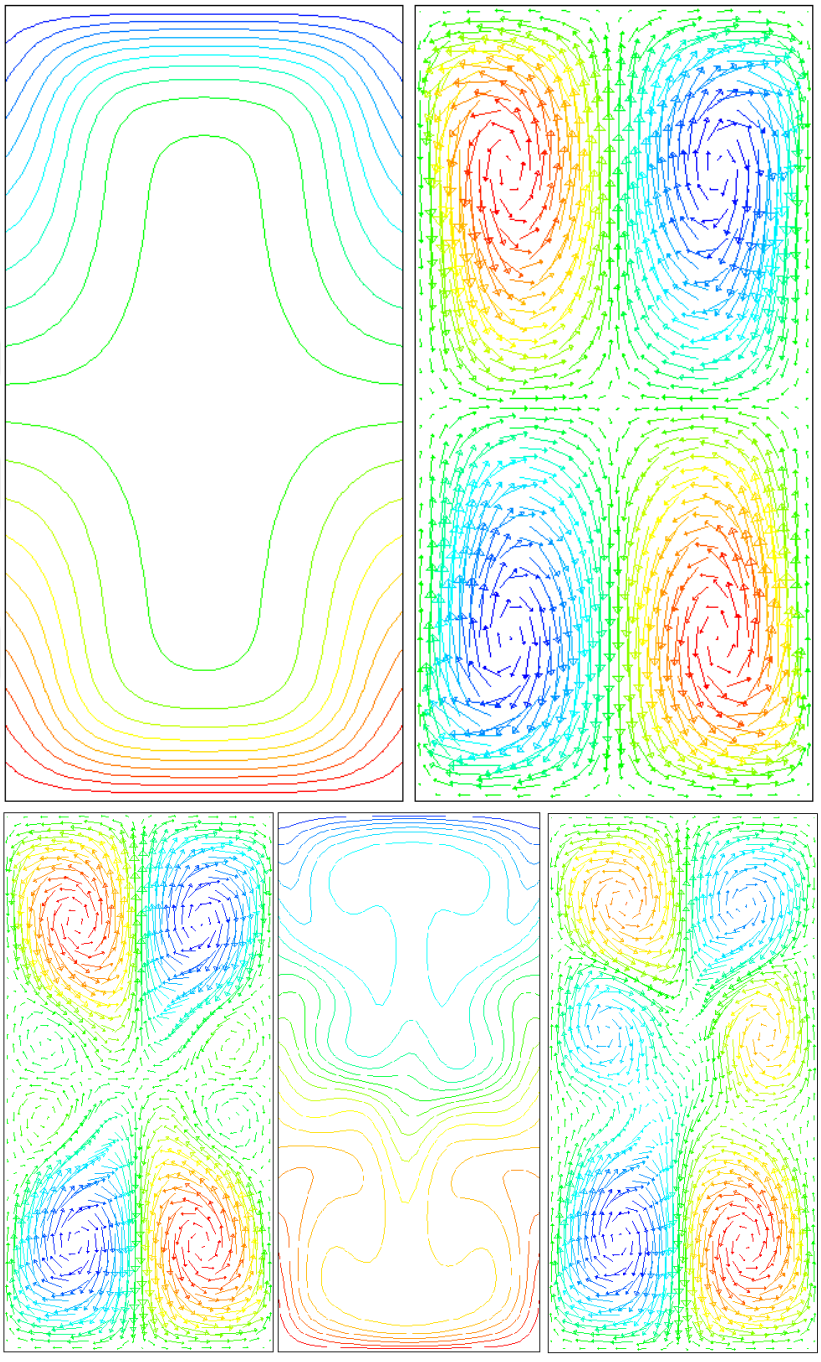

Figure 4.14. Temperature contours and velocity stream-function vectors at $Ra = 5 \times 10^5$ (first row) and $Ra = 2 \times 10^6$ (second row).

4.3. Multiple results in natural convection

The multiple results are discussed in this section for different ARs. The results can be multiple considering the direction of velocity stream line vectors, the number of convective cells, and the shape of flow patterns.

In Figure 4.15, the even number BCs are used as initial values (left), and the odd number BCs are used as initial values (right). In both cases, the boundary condition on side wall is insolated as Rayleigh-Benard problem. The multiple results are obtained in completely same parameters and conditions. The direction of velocity streamlines is opposite in this case.

At critical Ra number $Ra = 8 \times 10^4$ which is depicted in Figure 4.16, multiple results could be observed. By using Ra and BC continuation, the multiplicity phenomena in natural convection is observed.

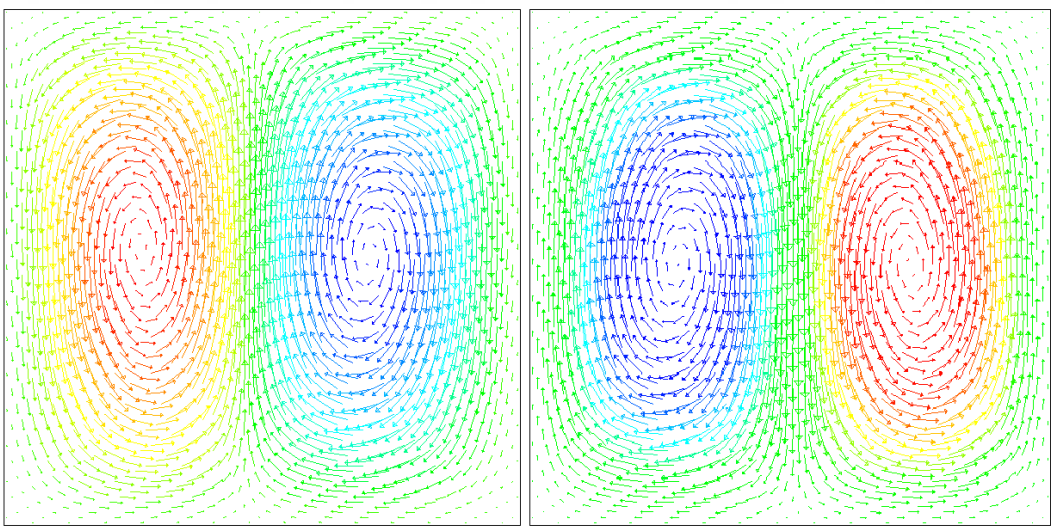

Figure 4.15. Velocity streamlines at $Ra = 1 \times 10^4, Pr = 1$, and same insulated BC.

In Figure 4.16 the even number BCs are used as initial value (top), and the odd number BCs are used as initial value (bottom). Here, the various BC initial values change the direction of velocity streamlines.

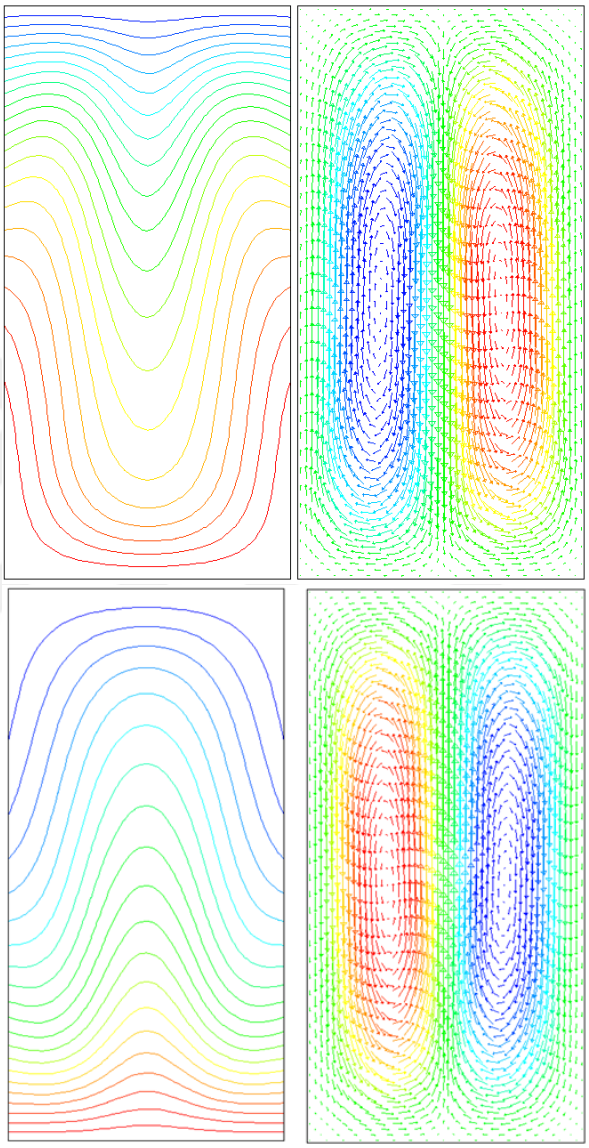

Figure 4.16. Temperature contours (left) and velocity streamlines (right); at $Ra = 8 \times 10^4$and Pr=1. In upper figures BC1 is performed on walls, and for the other ones the BC2 is used.

By increasing the iteration numbers, one result shifted to other result in which the direction of streamlines is changed as shown in Figure 4.17. In this figure, the first case from the left, the streamlines rise up from side walls and sink down from the middle of domain. However, the streamlines of right one is opposite of the left one. This phenomenon can be interpreted as a transition phenomenon between multiple results.

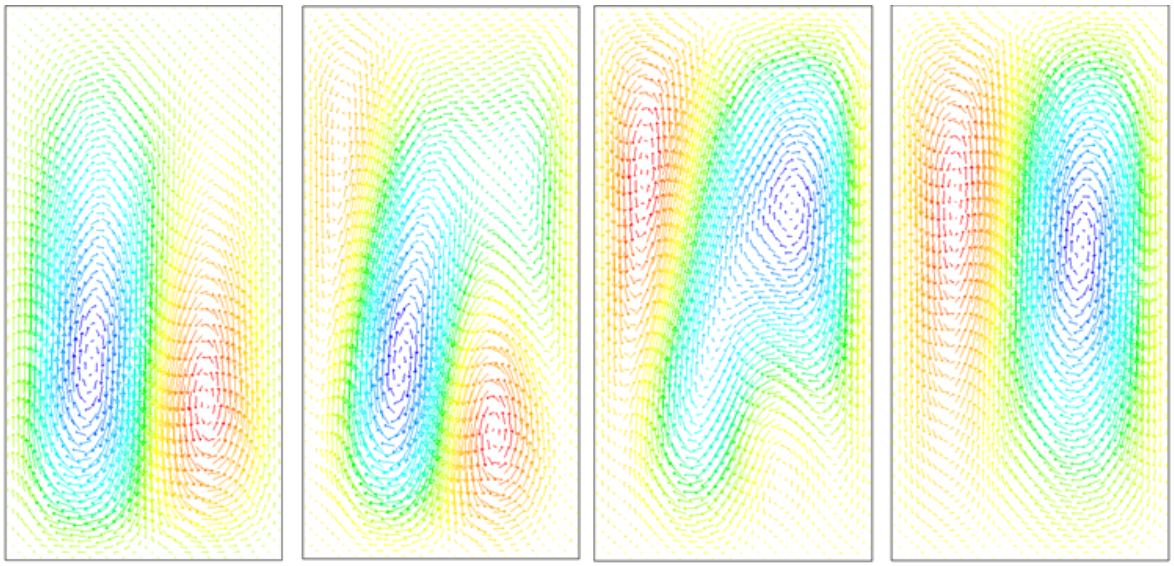

Figure 4.17. Change in the direction of the cells from left to right.

4.4. Comparison

Venturi et al. (2010) [1] observed the onset of instability i.e. transition from conduction to convection at Ra=2585. The one-roll convection pattern can be obtained at this Ra number in both directions (clockwise and counterclockwise) as shown in Figure 4.18(a). In this thesis, the onset of instability is observed at Ra=2700 and the one convection cell in both directions is shown in Figure 4.19 (a) and (b).

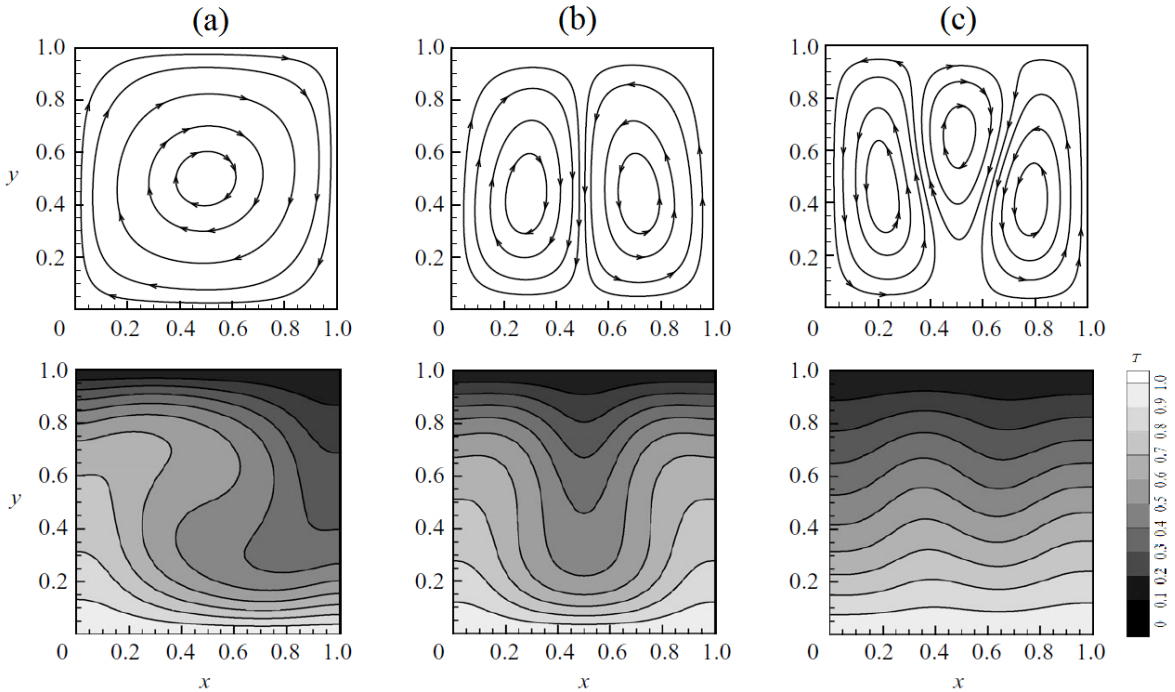

Figure 4.18. Velocity streamlines (first row) and temperature contours (second row) which are obtained by Venturi et al. (2010) [1]; a) one-roll convection pattern defined as $S^{\pm 1}$ (+ clockwise roll, − anticlockwise roll) at Ra = 15000 ; b) two-roll at Ra=15000 ; c) unstable three-roll convection pattern at Ra=21000.

The two-cell convection patterns are obtained using initial values at side-walls boundaries and the steady-state results in both direction are obtained in Figure 4.20. Venturi et al. [1] observed the secondary branch point as shown in Figure 4.18(b). This is in agreement with the results obtained in present study.

In this investigation, the third bifurcation point is happened at $Ra = 4 \times 10^4$ as shown in Figure 4.21 (a) and (b) in both directions. Two small cells appear at top

corners (Figure 4.21 (a)) and at bottom corners (Figure 4.21 (b)). The three-cell result obtained by Venturi et al. [1] at Ra=21000 is an unstable result. This is shown in Figure 4.18 (c). The result in the present work, however, is stable as shown in Figure 4.21 (a) and (b). By increasing Ra to $Ra = 8 \times 10^4$, four symmetric stable cells appear as illustrated in Figure 4.21 (c).

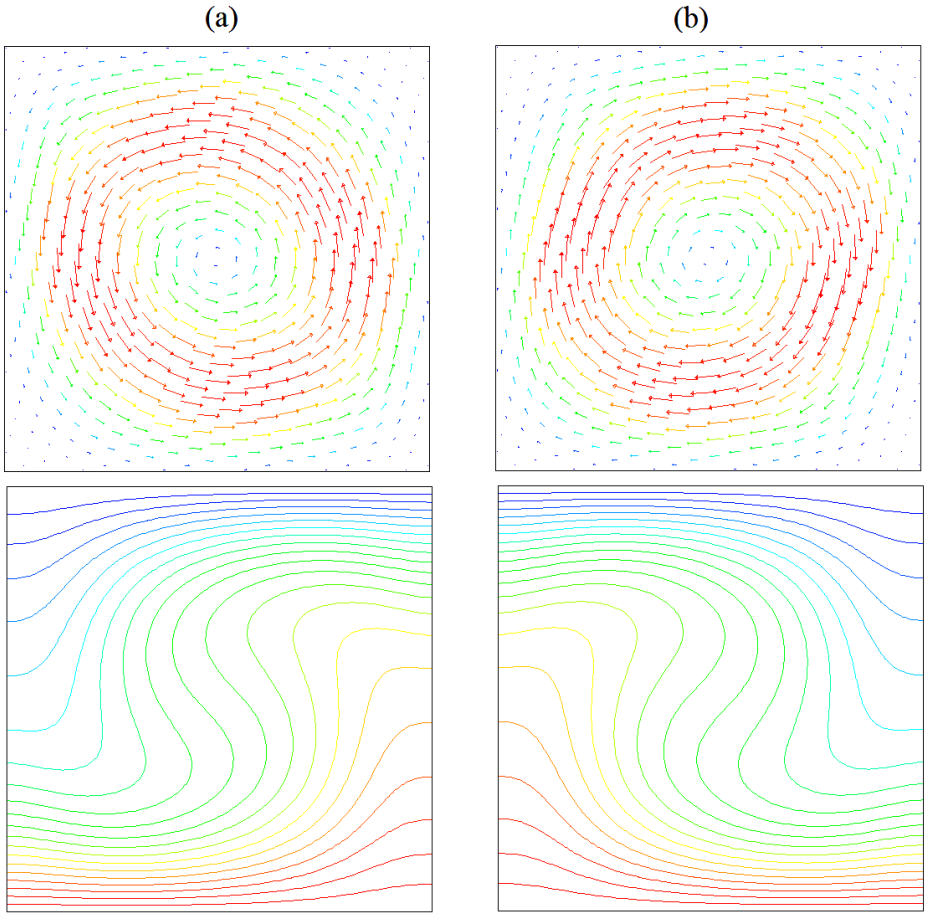

Figure 4.19. Velocity magnitude vectors and temperature contours AR=1, Ra=5000 and Pr=0.7 ; a) counterclockwise ; b) clockwise .

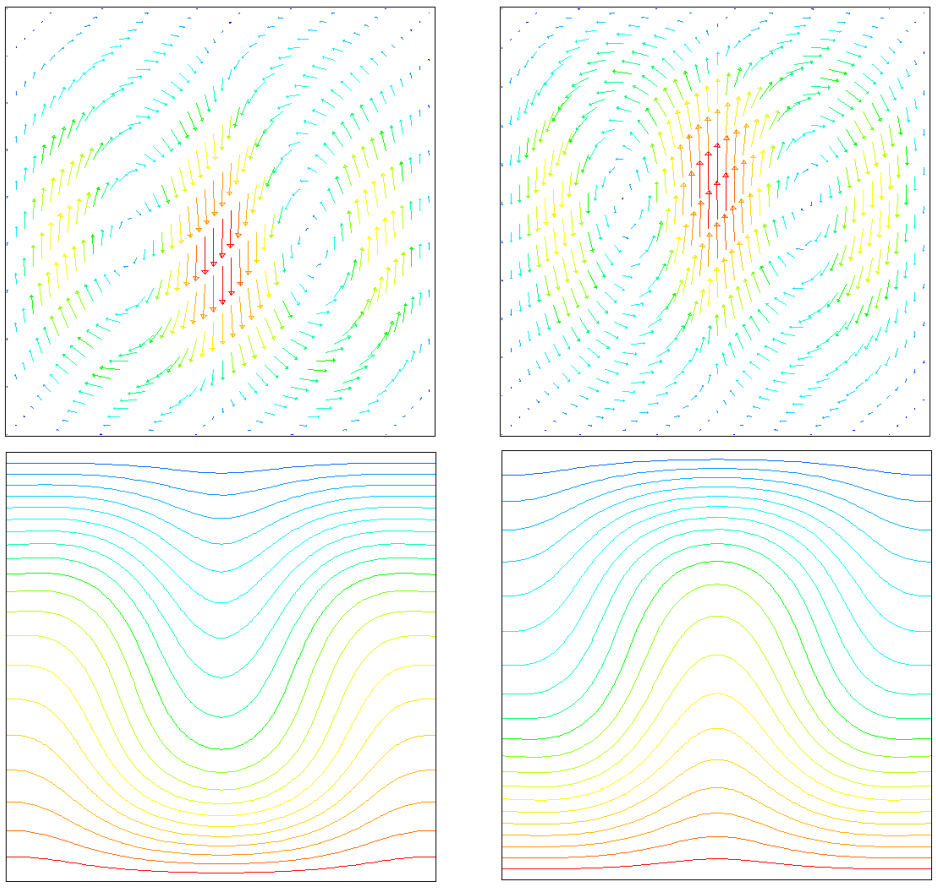

Figure 4.20. Velocity magnitude vectors and temperature contours for AR=1, $Ra = 1 \times 10^4$ and Pr=0.7; two-roll convection pattern in opposite directions.

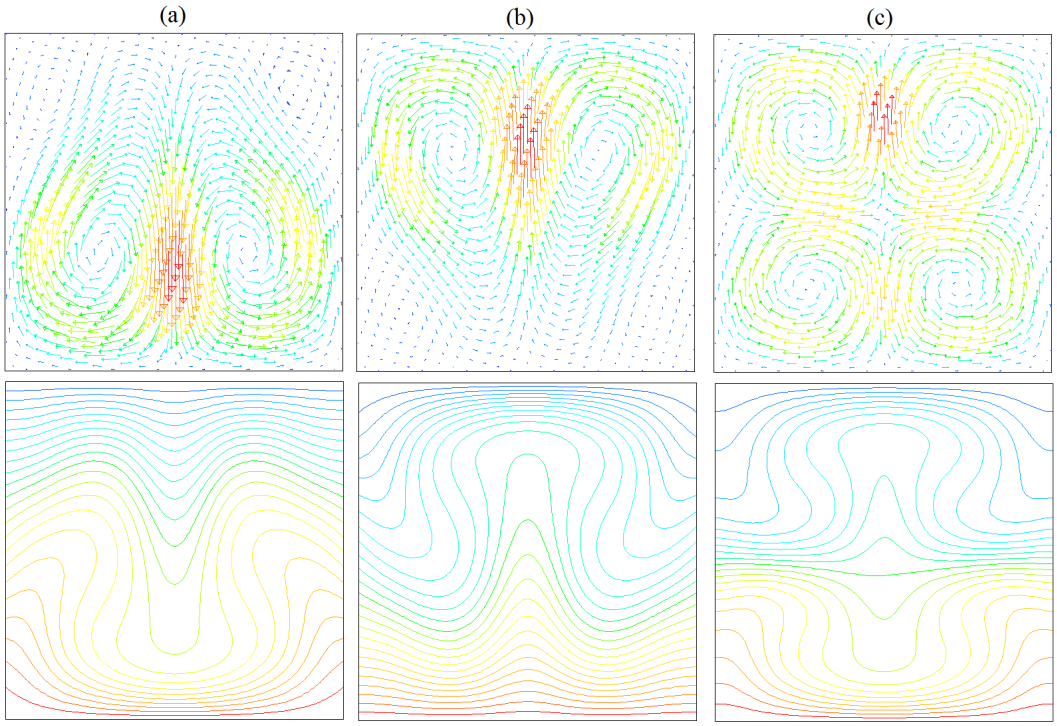

Figure 4.21. Velocity magnitude vectors and temperature contours; a) and b) four-roll stable patterns in opposite directions $Ra = 4 \times 10^4$; c) four symmetric stable cells at $Ra = 8 \times 10^4$.

Figure 4.22 shows the two unstable convection cells from the study by Puigjaner et al. (2004) [2]. This pattern is shown as S2 in their work. Similar simulations have been carried out here. The results are illustrated in Figure 4.22 which shows a good agreement with those obtained by Puigjaner et al. (2004) [2].

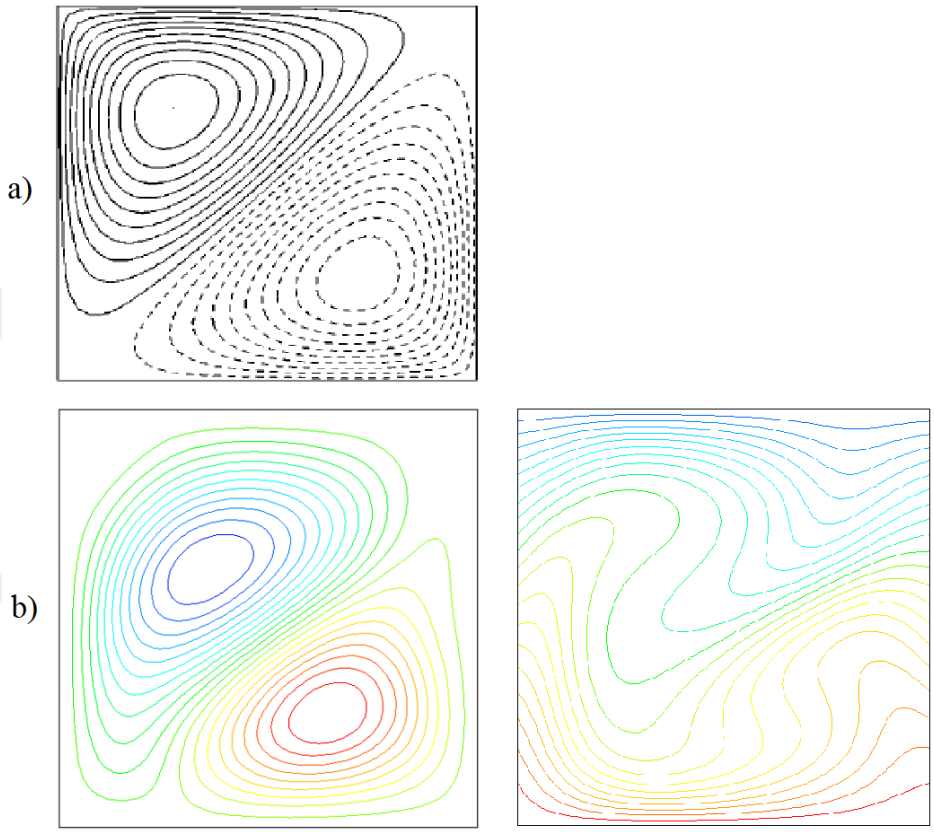

Figure 4.22. Unstable pattern of velocity stream-function; a) Puigjaner et al. (2004) [2] ; b) present study .

Figure 4.23 illustrates the variation of Nu number with Ra number for $Ra = 1700 - 10^4$. For comparison purposes, Figure 4.23 also presents the simulation results obtained by Bhattacharya [3] and those derived from the empirical formulation $Nu = 1.56 \times (Ra)^{1/4}$ [43]. In all 3 cases, AR=1/2, Pr=3 and the material properties are equal to material properties of water at $60°C$.

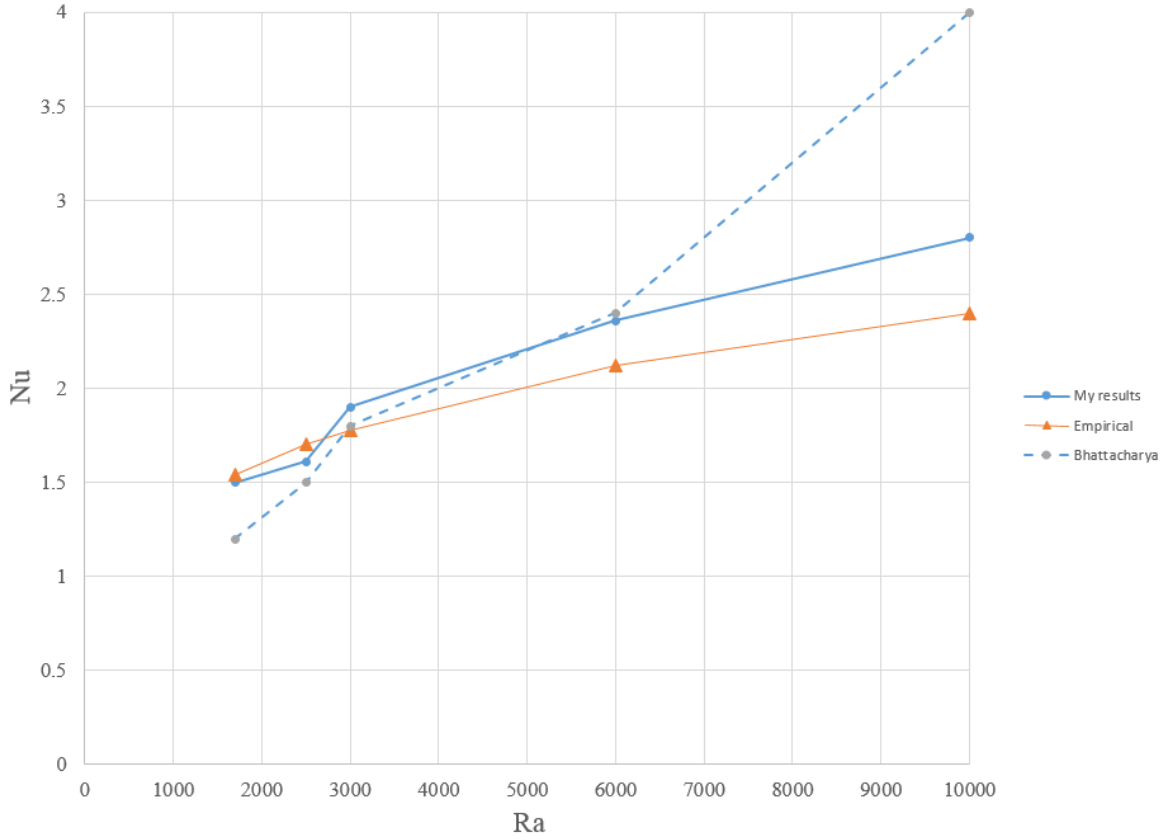

Figure 4.23. Comparison of Nu number between the present numerical results and the numerical results by Bhattacharya [3] and empirical results for Pr=3 and AR=1/2.

According to this plot, all three cases follow the same trend i.e. Nu increases by increasing Ra. Except for $Ra = 10^4$, the results are relatively close. In this Ra, however, Bhattacharya [3] predicts much higher Nu.

5. CONCLUSIONS

In this study, the transition and multiple results phenomena for natural convection are investigated. The BC and Ra continuation methods are implemented to find the onset of bifurcation and critical Ra numbers. Moreover, for large Ra numbers i.e. larger than first critical value, the pseudo-transient method is utilized to help the residuals to converge and stabilize unstable results.

First, a parametric analysis at different Ra numbers is carried out for constant AR = 1/2 and Pr = 5. The outcome reveals a range of critical Ra numbers for which transition phenomenon occurs. It is observed that increasing the Ra number causes the velocity magnitude and Nu number to increase. However, the rate of this increase is not significant in transition region. Then, more cases are investigated for the convection flow patterns at critical Ra numbers.

In second case, maximum value of the Nu number and velocity magnitude is obtained for a range of Pr numbers between 0.1 and 10 and at constant Ra = 2×10^5 and AR = 2. According to the results, by decreasing the Pr number from 10 to 0.1, the velocity magnitude is increased except for Pr=0.5 in which the magnitude of two kidney shape velocity cells is divided to four velocity cells that leads to a decrease in the velocity magnitude. At Pr=0.1, the velocity magnitude increases again. It can also be concluded that the critical Ra number increases with decreasing Pr number. Hence, at Pr=0.1 and Pr=0.5, four symmetric velocity cell exist (Figure 4.5). Indeed, the bifurcation point for transition from two-rolls to four-rolls for low Pr numbers(lower than one) occurs at low Ra number values in these cases as shown in Figure 4.5.

In third case, different ARs are considered with Ra = 8×10^4 and Pr=1. Maximum value of the Nu number and velocity magnitude are then obtained in each AR. Looking at Figure 4.7, one can notice that increasing the AR results in decreasing both velocity and Nu. It is concluded that increasing the AR results in decreasing both velocity and Nu. Four symmetric convective cells are observed at AR=1/4 and $Ra = 8 \times 10^4$ as

shown in Figure 4.8. The results are stable for cases with AR=1/2 and 1/4 (Figure 4.8 (a) and (b)). According to the results, the transition from two-cells to four-cells patterns occurs in AR=1 as shown in Figure 4.8 (c). It should be noted that the critical Ra number occurs in higher orders (10^5 and 10^6) for AR=2 and 4. Hence, two stable kidney shape cells are observed for these cases as shown in Figure 4.9 and 4.10. Finally, comparing Figures 4.8, 4.9 and 4.10, it can be interpreted that the critical Ra number increases with decreasing AR.

In all of the cases, behavior of convective flow changes significantly within the transition region. This can be explained by energy balance within the enclosure as studied in experimental research by Mishra et al. [40].

Multiple convection flow patterns are obtained. The multiple results are investigated considering the direction of velocity streamline vectors and the number and shape of convection flow patterns. In addition, the transition phenomenon between multiple results for the same parameters shows that one unstable result can be converted to other result.

The results in this thesis provide new areas of study for future work since it is concluded that the transition and multiplicity effects play a significant role in convection flow patterns within the closed domain.

REFERENCES

1. Venturi, D., X. Wan and G. E. Karniadakis, "Stochastic bifurcation analysis of Rayleigh–Bénard convection", *Journal of Fluid Mechanics*, Vol. 650, pp. 391–413, 2010.

2. Puigjaner, D., J. Herrero, F. Giralt and C. Simó, "Stability analysis of the flow in a cubical cavity heated from below", *Physics of Fluids (1994-present)*, Vol. 16, No. 10, pp. 3639–3655, 2004.

3. Bhattacharya, S., "Effect of Initial Condition and Influence of Aspect Ratio Change on Rayleigh-Benard Convection", .

4. Hurle, D., "Temperature oscillations in molten metals and their relationship to growth striae in melt-grown crystals", *Philosophical Magazine*, Vol. 13, No. 122, pp. 305–310, 1966.

5. Hsieh, Y.-F., D.-S. Lee, P.-H. Chen, S.-K. Liao, S.-H. Yeh, P.-J. Chen and A.-S. Yang, "A real-time convective PCR machine in a capillary tube instrumented with a CCD-based fluorometer", *Sensors and Actuators B: Chemical*, Vol. 183, pp. 434–440, 2013.

6. Zeytounian, R. K., "Joseph Boussinesq and his approximation: a contemporary view", *Comptes Rendus Mécanique*, Vol. 331, No. 8, pp. 575–586, Aug. 2003.

7. J., B., *Théorie Analytique de la Chaleur*, Vol. II, Gauthier-Villars, Paris, 1903.

8. Flemings, M. C., "Solidification processing", *Metallurgical Transactions*, Vol. 5, No. 10, pp. 2121–2134, 1974.

9. Müller, G. and A. Ostrogorsky, "Convection in melt growth", *Handbook of Crystal Growth*, Vol. 2, pp. 709–819, 1994.

10. Müller, A. and M. Wilhelm, "Periodische temperaturschwankungen in flüssigem InSb als ursache schichtweisen einbaus von Te in kristallisierendes InSb", *Zeitschrift für Naturforschung A*, Vol. 19, No. 2, pp. 254–263, 1964.

11. Winters, K., "A bifurcation analysis of oscillatory convection in liquid metals", *Numerical Simulation of Oscillatory Convection on Low-Pr Fluids*, pp. 319–326, Springer, 1990.

12. Wakitani, S., "Numerical study of three dimensional oscillatory natural convection at low Prandtl number in rectangular enclosures", *Journal of heat transfer*, Vol. 123, No. 1, pp. 77–83, 2001.

13. Henry, D. and M. Buffat, "Two-and three-dimensional numerical simulations of the transition to oscillatory convection in low-Prandtl-number fluids", *Journal of Fluid Mechanics*, Vol. 374, pp. 145–171, 1998.

14. Gelfgat, A. Y., P. Bar-Yoseph and A. Yarin, "On oscillatory instability of convective flows at low Prandtl number", *Journal of fluids engineering*, Vol. 119, No. 4, pp. 823–830, 1997.

15. GelFgat, A., P. Bar-Yoseph and A. Yarin, "Stability of multiple steady states of convection in laterally heated cavities", *Journal of Fluid Mechanics*, Vol. 388, pp. 315–334, 1999.

16. Danis, M., M. Orhan and A. Ecder, "ISPH modelling of transient natural convection", *International Journal of Computational Fluid Dynamics*, Vol. 27, No. 1, pp. 15–31, 2013.

17. Sheu, T. W., H. Rani, T.-C. Tan and S. Tsai, "Multiple states, topology and bifurcations of natural convection in a cubical cavity", *Computers & Fluids*, Vol. 37, No. 8, pp. 1011–1028, 2008.

18. Mercader, I., O. Batiste, L. Ramirez-Piscina, X. Ruiz, S. Rudiger and J. Casade-

munt, "Bifurcations and chaos in single-roll natural convection with low Prandtl number", *Physics of Fluids*, Vol. 17, No. 10, p. 104108, 2005.

19. Selver, R., Y. Kamotani and S. Ostrach, "Natural convection of a liquid metal in vertical circular cylinders heated locally from the side", *Journal of heat transfer*, Vol. 120, No. 1, pp. 108–114, 1998.

20. Yoo, J.-S., "Transition and multiplicity of flows in natural convection in a narrow horizontal cylindrical annulus: Pr= 0.4", *International journal of heat and mass transfer*, Vol. 42, No. 4, pp. 709–722, 1999.

21. Wei, J., L. Zheng and H. Zhang, "Suppression of melt convection in a proposed Bridgman crystal growth system", *International Journal of Heat and Mass Transfer*, Vol. 52, No. 15, pp. 3747–3756, 2009.

22. Rubinov, A., V. Erenburg, A. Y. Gelfgat, E. Kit, P. Bar-Yoseph and A. Solan, "Three-dimensional instabilities of natural convection flow in a vertical cylinder with partially heated sidewall", *Journal of heat transfer*, Vol. 126, No. 4, pp. 586–599, 2004.

23. Pulicani, J., E. C. Del Arco, A. Randriamampianina, P. Bontoux and R. Peyret, "Spectral simulations of oscillatory convection at low Prandtl number", *International Journal for Numerical Methods in Fluids*, Vol. 10, No. 5, pp. 481–517, 1990.

24. Hadid, H. B. and B. Roux, "Buoyancy-and thermocapillary-driven flows in differentially heated cavities for low-Prandtl-number fluids", *Journal of Fluid Mechanics*, Vol. 235, pp. 1–36, 1992.

25. Dixit, H. and V. Babu, "Simulation of high Rayleigh number natural convection in a square cavity using the lattice Boltzmann method", *International journal of heat and mass transfer*, Vol. 49, No. 3, pp. 727–739, 2006.

26. D'Orazio, A., M. Corcione and G. P. Celata, "Application to natural convection

enclosed flows of a lattice Boltzmann BGK model coupled with a general purpose thermal boundary condition", *International Journal of Thermal Sciences*, Vol. 43, No. 6, pp. 575–586, 2004.

27. Eggels, J. and J. Somers, "Numerical simulation of free convective flow using the lattice-Boltzmann scheme", *International Journal of Heat and Fluid Flow*, Vol. 16, No. 5, pp. 357–364, 1995.

28. Shu, C., Y. Peng and Y. Chew, "Simulation of natural convection in a square cavity by Taylor series expansion-and least squares-based lattice Boltzmann method", *International Journal of Modern Physics C*, Vol. 13, No. 10, pp. 1399–1414, 2002.

29. Hamimid, S., M. Guellal and M. Bouafia, "Numerical study of natural convection in a square cavity under non-boussinesq conditions", *Thermal Science*, , No. 00, pp. 84–84, 2014.

30. Vekstein, G., "Energy principle for the onset of convection", *European journal of physics*, Vol. 25, No. 5, p. 667, 2004.

31. Szewc, K., J. Pozorski and A. Taniere, "Modeling of natural convection with smoothed particle hydrodynamics: non-Boussinesq formulation", *International Journal of Heat and Mass Transfer*, Vol. 54, No. 23, pp. 4807–4816, 2011.

32. Mansour, A., A. Amahmid, M. Hasnaoui and M. Bourich, "Multiplicity of solutions induced by thermosolutal convection in a square porous cavity heated from below and submitted to horizontal concentration gradient in the presence of Soret effect", *Numerical Heat Transfer, Part A: Applications*, Vol. 49, No. 1, pp. 69–94, 2006.

33. Sezai, I. and A. Mohamad, "Double diffusive convection in a cubic enclosure with opposing temperature and concentration gradients", *Physics of Fluids (1994-present)*, Vol. 12, No. 9, pp. 2210–2223, 2000.

34. Booker, V. B., "An experimental and three-dimensional numerical investigation of

the Czochralski solidification of single silicon crystals", , 1997.

35. Yang, T. and L. Wang, "Bifurcation and stability of combined free and forced convection in rotating curved ducts of square cross-section", *International journal of heat and mass transfer*, Vol. 46, No. 4, pp. 613–629, 2003.

36. Zhang, J., B. Zhang and J. Jü, "Fluid flow in a rotating curved rectangular duct", *International Journal of Heat and fluid flow*, Vol. 22, No. 6, pp. 583–592, 2001.

37. Fluent, A., "ANSYS FLUENT Theory Guide: Version 13.0", *Ansys Inc, Canonsburg*, 2010.

38. Mousa, M., "Modeling of Laminar Buoyancy Convection in a Square Cavity Containing an Obstacle", .

39. Sreenivas, K., O. Singh and J. Srinivasan, "On the relationship between finger width, velocity, and fluxes in thermohaline convection", *Physics of Fluids (1994-present)*, Vol. 21, No. 2, p. 026601, 2009.

40. Mishra, D., K. Muralidhar and P. Munshi, "Experimental study of Rayleigh–Benard convection at intermediate Rayleigh numbers using interferometric tomography", *Fluid dynamics research*, Vol. 25, No. 5, pp. 231–255, 1999.

41. Fluent, A., "12.0 Theory Guide", *Ansys Inc*, Vol. 5, 2009.

42. Patankar, S. V. and D. B. Spalding, "A calculation procedure for heat, mass and momentum transfer in three-dimensional parabolic flows", *International Journal of Heat and Mass Transfer*, Vol. 15, No. 10, pp. 1787–1806, 1972.

43. Kao, P.-H. and R.-J. Yang, "Simulating oscillatory flows in Rayleigh–Benard convection using the lattice Boltzmann method", *International Journal of Heat and Mass Transfer*, Vol. 50, No. 17, pp. 3315–3328, 2007.